Master's Thesis

Understanding of Individual and Interconnected Actions of Pathological Features in Alzheimer's Disease

Eunju Nam
Department of Chemistry
Graduate School of UNIST
2017

Understanding of Individual and Interconnected Actions of Pathological Features in Alzheimer's Disease

A thesis submitted to the Graduate School of UNIST
in partial fulfillment of the requirements
for the degree of Master of Science

Eunju Nam

12. 09. 2016
Approved by

Advisor
Associate Professor Mi Hee Lim

Understanding of Individual and Interconnected Actions of Pathological Features in Alzheimer's Disease

This certifies that the thesis of Eunju Nam is approved

12.09.2016

Signature

Advisor: Associate Professor Mi Hee Lim

Signature

Assistant Professor Jung-Min Kee

Signature

Assistant Professor Hyun-Woo Rhee

Abstract

Alzheimer's disease (AD) is a fatal neurodegenerative disease which has symptoms related to memory loss and cognitive impairment. AD can be categorized as a protein misfolding disease, since abnormal accumulation and aggregation of amyloid-β (Aβ) peptides in the AD-affected brain are associated with neurotoxicity. Moreover, additional pathological features (*e.g.*, metal ion dyshomeostasis, oxidative stress) also exist and are indicated to interact with Aβ leading to AD pathogenesis. For instance, upon binding of redox-active metal ions with Aβ, facilitation of Aβ aggregation, including generation of toxic oligomer species, and production of reactive oxygen species (ROS) are observed. The interconnections that affect various microenvironments in cellular systems, which in turn cause neuronal death, have hindered the identification of AD etiology. Therefore, the determination of an inter-relationship among multiple pathological factors in AD pathology would provide a better understanding of AD etiology. The work presented in this dissertation focuses on this goal. In Chapter 1, the assembly of Aβ and detailed characterization of Aβ oligomers, proposed to be primary toxic species, are introduced. The toxicity mechanisms of Aβ oligomers in cellular systems as well as effective inhibitors against Aβ aggregation, including oligomerization, are also presented. In Chapter 2, the investigations of the inter-relationship between multiple pathological features (*e.g.*, Aβ, metals, metal-bound Aβ, ROS) and a neurotransmitter, dopamine, toward AD pathogenesis are described. The direct or indirect regulatory activities of dopamine against the pathological features *via* its oxidative transfigurations are observed, which provides advanced information on the role of the neurotransmitter in AD pathogenesis. Finally, in Chapter 3, our studies of fluorescent sensors for metal ions in living cells are reported. This work might be helpful to further probe metals' pathology in AD. Collectively, our work presented in this thesis illustrates a greater understanding and a better insightful view of AD pathology, which could be utilized for development of potential therapeutic agents for this disease.

Table of Contents

List of Tables

List of Figures

Figure 2.1. Inhibitory effects of **DA** on both metal-free and metal-induced Aβ aggregation in the presence and absence of O_2. (a) Scheme of inhibition experiments. (b) Visualization of the size-distribution of the resultant Aβ species with and without **DA** treatment under aerobic (top) and anaerobic (bottom) conditions. (c) TEM images of the resultant metal-free $A\beta_{42}$ and metal–$A\beta_{42}$ aggregates from the 24 h incubated samples. The scale bar is 500 nm. Experimental conditions: [$A\beta_{40}$ or $A\beta_{42}$] = 25 μM; [$ZnCl_2$ or $CuCl_2$] = 25 μM; [**DA**] = 50 μM; pH 6.6 (for Cu(II) samples) or pH 7.4 (for metal-free and Zn(II) samples); 37 °C; 24 h incubation; constant agitation.

Figure 2.2. Capability of **DA** to disaggregate preformed metal-free and metal-treated Aβ aggregates. (a) Scheme of disaggregation experiments. (b) Visualization of the size-distribution of $A\beta_{40}$ (left) and $A\beta_{42}$ (right) species with and without **DA** treatment. Experimental conditions: [$A\beta_{40}$ or $A\beta_{42}$] = 25 μM; [$ZnCl_2$ or $CuCl_2$] = 25 μM; [**DA**] = 50 μM; pH 6.6 (for Cu(II) samples) or pH 7.4 (for metal-free and Zn(II) samples); 37 °C; 24 h incubation; constant agitation.

Figure 2.3. Mass spectrometric analyses of $A\beta_{40}$ monomers treated with **DA**. The addition of an oxygen atom is marked in a red dot. (a) Mass spectrometric analysis showing $A\beta_{40}$ oxidation in the presence of **DA**. (b) Arrival time distribution (ATD) of the singly oxidized $A\beta_{40}^{4+}$ peak $[A\beta_{40} + O + 4H]^{4+}$. Collision cross section (CCS) values for all ion mobility data sets are presented in Table 2.1. (c) Mass spectrometric analysis of $A\beta_{40}$ monomers with **DA** and $CuCl_2$. (d) MS/MS sequencing of the oxidized $A\beta_{40}^{4+}$ peak $[A\beta_{40} + O + 4H]^{4+}$. Experimental conditions: [$A\beta_{40}$] = 100 μM; [$CuCl_2$] = 100 μM; [compound] = 500 μM; pH 7.5; 37 °C; 6 h incubation (for metal-free samples) or 1 h incubation (for Cu(II) samples); 100 mM ammonium acetate. Incubated samples were diluted by 10-fold before injection into the mass spectrometer.

Figure 2.4. Oxidative transformations of **DA**. (a) Electrochemical analysis of **DA**. Cyclic voltammograms of **DA** in H_2O with 1 M NaCl as a supporting electrolyte at variable scan rates (5, 10, 25, 50, 100, 150, 200, 250, and 300 mV/s). (b) Spectroelectrochemical investigations of **DA** (0.627 V). Potentials were reported and collected *versus* the Ag/AgCl couple. (c) Transformations of **DA** with or without $CuCl_2$ and/or $A\beta_{40}$, monitored by UV-vis spectroscopy. Experimental conditions: [$A\beta_{40}$] = 50 μM; [$CuCl_2$] = 50 μM; [compound] = 100 μM, pH 6.6 (for Cu(II) samples) or pH 7.4 (for metal-free samples); 37 °C; 1 h incubation; no agitation. (d) **DA's** transfigurations with or without $CuCl_2$ and/or $A\beta_{40}$ measured by mass spectrometry. Experimental conditions: [$A\beta_{40}$] = 100 μM; [$CuCl_2$] = 100 μM; [compound] = 500 μM; 100 mM ammonium acetate; pH 7.5; 37 °C; 1 h incubation; no agitation. Incubated samples were diluted by 10-fold before injection into the mass spectrometer.

Figure 2.5. Derivatives of **DA**. The catechol moiety (Site I) was systematically altered to monomethoxy or dimethoxy functionality. The primary amino group of **DA** (Site II) was varied with a monomethylamino or dimethylamino group.

Figure 2.6. Cyclic voltammograms of **DA**'s derivatives in H_2O with 1 M NaCl as a supporting electrolyte at variable scan rates (5, 10, 25, 50, 100, 150, 200, 250, and 300 mV/s).

Figure 2.7. Transformations of **2**, **3**, and **4** with or without $CuCl_2$ and/or $A\beta_{40}$, monitored by UV-vis spectroscopy. UV-vis spectra of **2**, **3**, and **4** with or without $CuCl_2$ in the absence (a, b) or presence of $A\beta_{40}$ (c, d) were measured. Experimental conditions: [$A\beta_{40}$] = 50 μM; [$CuCl_2$] = 50 μM; [compound] = 100 μM, pH 6.6 (for Cu(II) samples) or pH 7.4 (for metal-free samples); 37 °C; 1 h incubation; no agitation.

Figure 2.8. Transformation of **2**, **3**, and **4** with or without $CuCl_2$ and/or $A\beta_{40}$, monitored by mass spectrometry. Experimental conditions: [$A\beta_{40}$] = 100 μM; [$CuCl_2$] = 100 μM; [compound] = 500 μM; 100 mM ammonium acetate; pH 7.5; 37 °C; 1 h incubation; no agitation. The incubated samples were diluted by 10-fold before injection into the mass spectrometer.

Figure 2.9. Capacity of **DA** derivatives to control metal-free and metal-induced Aβ aggregation. (a) Scheme of inhibition experiments. (b) Visualization of the size distribution of the resultant Aβ species in the absence or presence of **DA** derivatives (c) TEM images of the resultant metal-free and metal-induced Aβ aggregates from the 24 h incubated samples. The scale bar is 500 nm. Experimental conditions: [$A\beta_{40}$ or $A\beta_{42}$] = 25 μM; [$CuCl_2$] = 25 μM; [compound] = 50 μM; pH 6.6 (for Cu(II) samples) or pH 7.4 (for metal-free samples); 37 °C; 24 h incubation; constant agitation.

Figure 2.10. Mass spectrometric analyses of $A\beta_{40}$ monomers treated with **3** and **4** in the absence or presence of Cu(II). The addition of an oxygen atom is marked in a red dot. Experimental conditions: [$A\beta_{40}$] = 100 μM; [$CuCl_2$] = 100 μM; [compound] = 500 μM; pH 7.5; 37 °C; 6 h incubation (for metal-free samples) or 1 h incubation (for Cu(II) samples); 100 mM ammonium acetate. The incubated samples were diluted by 10-fold before injection into the mass spectrometer.

Figure 2.11. MS/MS sequencing of the oxidized $A\beta_{40}^{4+}$ peak $[A\beta_{40} + O + 4H]^{4+}$. Experimental conditions: [$A\beta_{40}$] = 100 μM; [compound] = 500 μM; pH 7.5; 37 °C; 6 h incubation; 100 mM ammonium acetate. The incubated samples were diluted by 10-fold before injection into the mass spectrometer.

Figure 3.1. Fluorescent responses of **A** to Al (III) in HeLa cells. Cells were exposed to (a) 0 and (b) 300 μM Al(III) for 4 h prior to addition of **A** (10 μM). Experimental conditions: 37 °C; 5% CO_2. The scale bar is 100 μm. The DAPI light cube [DAPI, 2-(4-Amidinophenyl)-1*H*-indole-6-carboxamidine; excitation 357 (± 22) nm; emission 447 (± 30) nm] was employed to perform imaging experiments.

Figure 3.2. Fluorescent responses of **B** to Hg(II) in HeLa cells. Cells were pre-incubated with **B** for 5 min prior to addition of various concentrations of Hg(II). Experimental conditions: [Hg(II)] = 0, 10, 20, 30, 40, and 50 μM; [**B**] = 5 μM; 37 °C; 5% CO_2. The scale bar is 50 μm. The GFP light cube [excitation 470 (±11) nm; emission 510 (±21) nm] was used to detect the fluorescence.

Figure 3.3. Fluorescent responses of **C** to Al(III) in HeLa cells. Cells were exposed to (a and b) 0 or (c-f) 100 μM Al(III) for 1 h prior to addition of **C** (20 μM). (a and c) Bright-field images of cells without or with Al(III), respectively. Fluorescent responses to Al(III) were detected in the (b) absence or (d) presence of Al(III). To investigate the distribution of fluorescence, (e) the nuclei of cells were stained with **SYTO16** (2.5 μM). (f) Overlapped fluorescence images of (d) and (e). Experimental conditions: DAPI channel [λ_{ex} = 357 (± 22) nm; λ_{em} = 447 (± 30) nm] for (b) and (d); GFP channel [excitation 470 (±11) nm; emission 510 (±21) nm] for (e). The scale bar is 25 μm.

List of Schemes

List of Abbreviations

α7 nAChR	α7 Nicotinic acetylcholine receptor
Aβ	Amyloid-β
AD	Alzheimer's disease
AFM	Atomic force microscopy
AMPA	α-Amino-3-hydroxy-5-methyl-4-isoxazolepropionate
APP	Amyloid precursor protein
BBB	Blood-brain barrier
BD-Oligo	BoDipy-Oligomer
BMAOIs	Bivalent multifunctional amyloid-β oligomerization inhibitors
Cryo-EM	Cryo-electron microscopy
CV	Cyclic voltammetry
DA	Dopamine
DAPI	2-(4-Amidinophenyl)-1*H*-indole-6-carboxamidine
DMPD	*N*,*N*-Dimethyl-*p*-phenylenediamine
DMSO	Dimethyl sulfoxide
Drp1	Dynamin-related protein 1
D-Trp-Aib	D-Tryptophan linked with α-aminoisobutyric acid
EGCG	(–)-Epigallocatechin gallate
EM	Electron microscopy
eNMDAR	Extrasynaptic *N*-methyl-D-aspartate receptors
ER	Endoplasmic reticulum
ESI-MS	Electrospray ionization mass spectrometry
FA	Ferulic acid
Gammabodies	Grafted AMyloid-Motif AntiBODIES
IDP	Intrinsically disordered protein

IM-MS	Ion mobility mass spectrometry
LTP	Long-term potentiation
MD	Molecular dynamics
Met	Methionine
MS	Mass spectrometry
MW	Molecular weight
NDGA	Nordihydroguaiaretic acid
NMDA	*N*-Methyl-D-aspartate
NMR	Nuclear magnetic resonance
PAGE	Polyacrylamide gel electrophoresis
ProSP-C	Prosurfactant protein C precursor
PrP^c	Cellular prion protein
RA	Rosmarinic acid
ROS	Reactive oxygen species
SAXS	Small angle X-ray scattering
SEC	Size exclusion chromatography
TEM	Transmission electron microscopy

Chapter 1.

Towards an Understanding of Amyloid-β Oligomers: Characterization, Toxicity Mechanisms, and Inhibitors

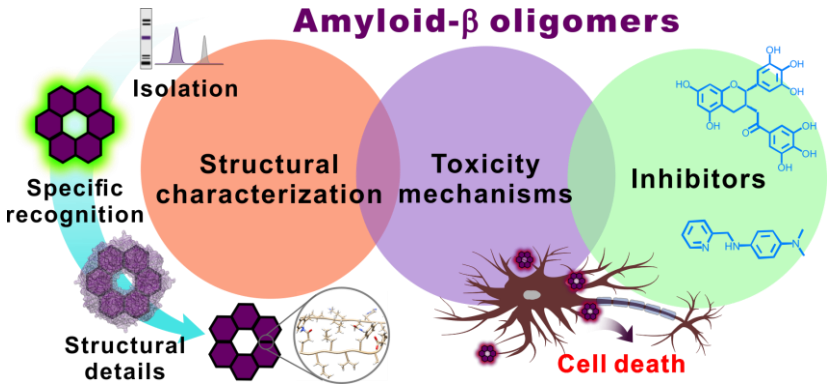

This chapter was recently published in *Chem. Soc. Rev* as a tutorial review. I was involved in writing of this review article, along with Shin Jung C. Lee, Hyuck Jin Lee, and Masha G. Savelieff. I thank Professor Lim for her guidance throughout the writing of this review article.

Shin Jung C. Lee,[†] Eunju Nam,[†] Hyuck Jin Lee, Masha. G. Savelieff, and Mi Hee Lim, Towards an understanding of Amyloid-β Oligomers: Characterization, Toxicity Mechanisms, and Inhibitors, *Chem. Soc. Rev.*, **2017**, In Press (DOI: 10.1039/C6CS00731G)([†] Co-first authorship).

1.1. Introduction

Alzheimer's disease (AD) is a fatal neurodegenerative disorder in the brain.[1] One explanation regarding AD pathogenesis is the amyloid cascade hypothesis, first put forward by Hardy and Higgins, which postulates that amyloid-β (Aβ) aggregation and accumulation cause neuronal death leading to AD.[2] The amyloid cascade hypothesis was challenged by the observation that neuronal injury did not necessarily occur where Aβ plaques were deposited.[3] This discrepancy, however, was reconciled by multiple reports which demonstrated that the neurotoxic effects could instead be attributed to soluble and diffusive Aβ oligomers.[4] Even in the absence of mature fibers, oligomeric species were sufficient to induce toxicity and neuronal death in AD mouse models.[5,6]

Significant efforts have been made to gain a molecular-level understanding of Aβ oligomers' assembly, structural characteristics, and interactions with other biomolecules, such as proteins and membranes, to identify how they could trigger toxicity.[7-12] Unfortunately, since Aβ oligomers consist of a heterogeneous combination of polymorphic intermediates generated by multiple pathways, it has been challenging to characterize their structures and properties.[7] Despite obstacles, recent progress in biophysical and biochemical methods has overcome intrinsic difficulties in investigating Aβ oligomers. In addition, the characterization and recognition of specific oligomeric species in the extracellular environment and within cellular compartments have suggested mechanisms of Aβ oligomers' toxicity.[8,11] Prion-like cell-to-cell transmission of Aβ oligomers might also be one mechanism by which Aβ oligomers' toxicity could spread.[13] Moreover, some approaches to modulate the formation and presence of Aβ oligomers have been developed to elucidate their roles in amyloid-related diseases and discover effective diagnostics and therapeutics.[14,15] Herein, we review the current body of knowledge on the assembly mechanisms and structural properties of Aβ oligomers, as well as pathways by which they might induce and transmit toxicity. The remaining part of the review describes on some chemical agents (*e.g.*, natural products, synthetic compounds, and peptide/protein domains) that can control Aβ aggregation, including oligomers' formation or disaggregation, towards a potential therapeutic avenue.

1.2. Assembly Pathways of Aβ Oligomers

An amyloid is a type of protein which is susceptible to structural conversion and assembly into cross-β-structured fibrils.[1] Amyloid protein aggregation is considered a hallmark in several degenerative disorders (*e.g.*, AD, Parkinson's disease, Huntington's disease, type II diabetes, and transmissible spongiform encephalopathy).[1] In the case of AD, it is characterized by multiple pathogenic features, one of which is the presence of Aβ plaques in AD patients' brain tissue.[1,2] Aβ peptides are produced by proteolytic cleavage of the hydrophobic transmembrane portion of the amyloid precursor protein (APP) by β- and γ-secretases (Figure 1.1a).[2] They are generated in several isoforms (especially, two

$A\beta_{40}$ and $A\beta_{42}$ isoforms are the major constituents of amyloid plaques found in AD patients' brains). The difference of only two amino acids between $A\beta_{40}$ and $A\beta_{42}$ peptides at their C-terminals results in distinct aggregation and toxicity profiles.[16,17]

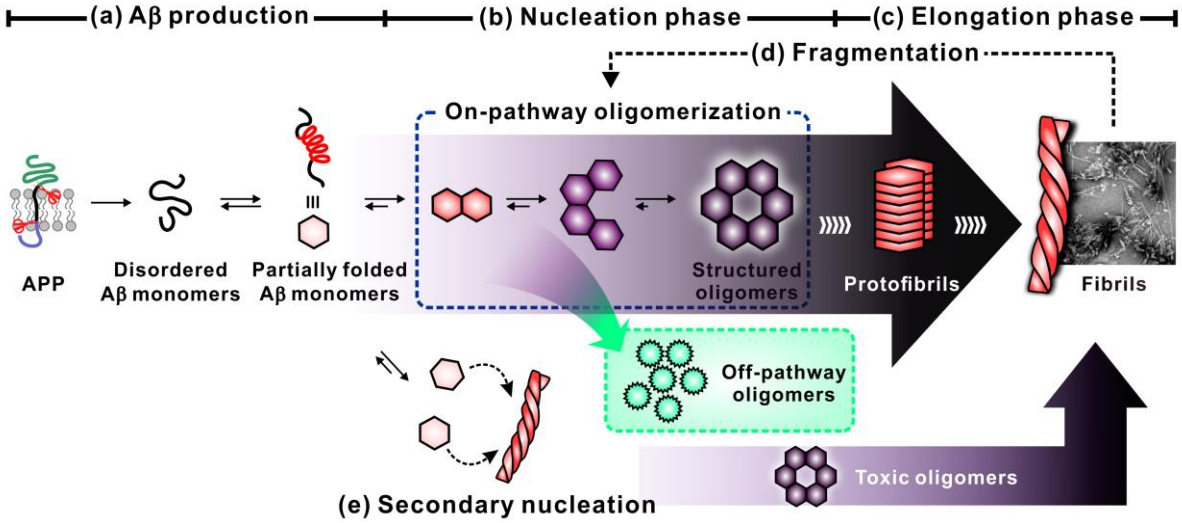

Figure 1.1. Schematic description of Aβ production and aggregation. (a) Aβ peptides are generated by sequential cleavage of APP by β- and γ-secretases. Aβ peptides are natively unfolded; however, due to environmental or genetic factors, they can be transformed into partially folded conformations. (b) Upon on-pathway oligomerization, Aβ forms structured, transient oligomers which are suspected to be toxic. Different types of oligomers, produced *via* off-pathway fibrillization, are also observed and stabilized without further fibril growth. (c) These structured oligomeric species are metastable intermediates that are transformed into protofibrils or fibrils. (d and e) Even after the structural transition into fibrils, some fibrils can fragment and reassemble into structured oligomeric species (fragmentation). In addition, structured oligomers can be generated through interactions between monomers and fibrils (secondary nucleation).

Aβ peptides are natively disordered (that is, they do not have stabilized secondary or tertiary structures). Still, they experience conformational fluctuations which can lead to folded or partially states.[1,7] The presence of external factors (*e.g.*, pH, temperature, peptide concentration, and interactions with other molecules) or genetic mutations (*e.g.*, amino acid substitutions) may also prompt protein folding.[1,7] Partially folded Aβ monomers are prone to interact with one another by contacts at their self-recognition sites, which initiates aggregation (Figure 1.1b).[1,7] The intermolecular interactions between Aβ peptides are sufficient to overcome unfavorable entropical changes; thus, amyloid oligomerization is a spontaneous process.[1] In the early stages of oligomerization, small oligomeric assemblies, suspected to be toxic, generate a nucleus which readily leads to the formation of larger aggregates (Figure 1.1b).

The polymorphic Aβ species (*i.e.*, species possessing a distinct arrangement of Aβ units into diverse three-dimensional structures) that form during the nucleation phase are called on-pathway

oligomers and they transform into larger aggregates or β-strand fibrils (Figure 1.1b).[1,7] On the other hand, there are different species which deviate from the principal aggregation/fibrillation pathways which are termed off-pathway oligomers (indicated by the green box in Figure 1.1). Off-pathway oligomers are distinguishable from on-pathway oligomers, and are generally regarded as unstructured and nontoxic.[14] Therefore, these amorphous off-pathway species are not recognized by conformational antibodies which are specific towards toxic structured oligomers.[14] Moreover, off-pathway oligomers can be stable final products rather than intermediates,[14] in contrast to on-pathway oligomers which are transient and transition to protofibrils and fibrils during the elongation phase (Figure 1.1c).

Initially, oligomerization and aggregation occur from a pool of Aβ monomers by a process called primary nucleation (Figure 1.1b).[18] Another aggregation pathway is directed by heterogeneous contacts between monomers and fibrils (secondary nucleation; Figure 1.1e).[18] The nucleation phase (Figure 1.1b) is considered the rate-limiting step during amyloid fibrillation;[1] however, it is significantly shortened in secondary nucleation since interactions of monomers with fibrils could catalyze oligomerization.[18] In addition, although mature fibrils are relatively stable, they can still dissociate into small oligomers, due to shear forces, thus contributing to the pool of oligomers (fragmentation; Figure 1.1d).[18]

One recent study indicated that secondary nucleation and fibril fragmentation are in a positive feedback loop.[18] This means that fragmentation of fibrillar species raises the amount of oligomeric aggregates which seed further aggregation and affect secondary nucleation. Fibril fragmentation of mutant-rich domains, such as the Dutch mutant of Aβ, Aβ(16-22)(E22Q), could catalyze a progressive assembly pathway through conformational transitions.[19] It was shown that secondary nucleation overwhelms primary nucleation as a source for new oligomers/aggregates when a critical concentration of Aβ fibrils is attained (approximately a few tens of nanomolar concentration).[18,19] Thus, secondary nucleation coupled with fibril fragmentation significantly contributes to the proliferation of toxic species,[18] in a cascading series of aggregation processes that increase the amount of oligomeric and fibrillar Aβ at the expense of nontoxic monomers. The rising level of toxic, structured Aβ oligomers exacerbates AD pathology and accelerates neurodegeneration. In light of the role structured Aβ oligomers might have in AD pathogenesis, the clarification of their structures and toxicity mechanisms has become intensive areas of research as discussed in the next two sections.

1.3. Structural Characterization of Aβ Oligomers

Although Aβ aggregation has been relatively well documented, the precise nature of toxic agents in AD remains unknown. To address this aspect, a structure-toxicity relationship of Aβ oligomers needs to be revealed. Numerous characterization studies have currently shed light on the structural properties of Aβ oligomers. The difficulties faced by characterization investigations are inherent to the

characteristics of Aβ oligomers which are transient and readily convert into other conformations during amyloid oligomerization and fibrillation (Figure 1.1).[1,7] This results in a heterogeneous population of polymorphic, metastable Aβ oligomers; therefore, structural characterization techniques that can isolate species from complex mixtures or discern the diverse states from an ensemble are necessary.[7-12] Recently, in addition to identifying the nature and size of the toxic species and intermediate forms, advances in structural characterization methods have provided at the topological[16,17] and atomic level[20-22] structural insight into Aβ oligomers. This section briefly outlines the structural and conformational properties of Aβ oligomers and aggregation intermediates at various levels of resolution by multiple analytical tactics (Figure 1.2).

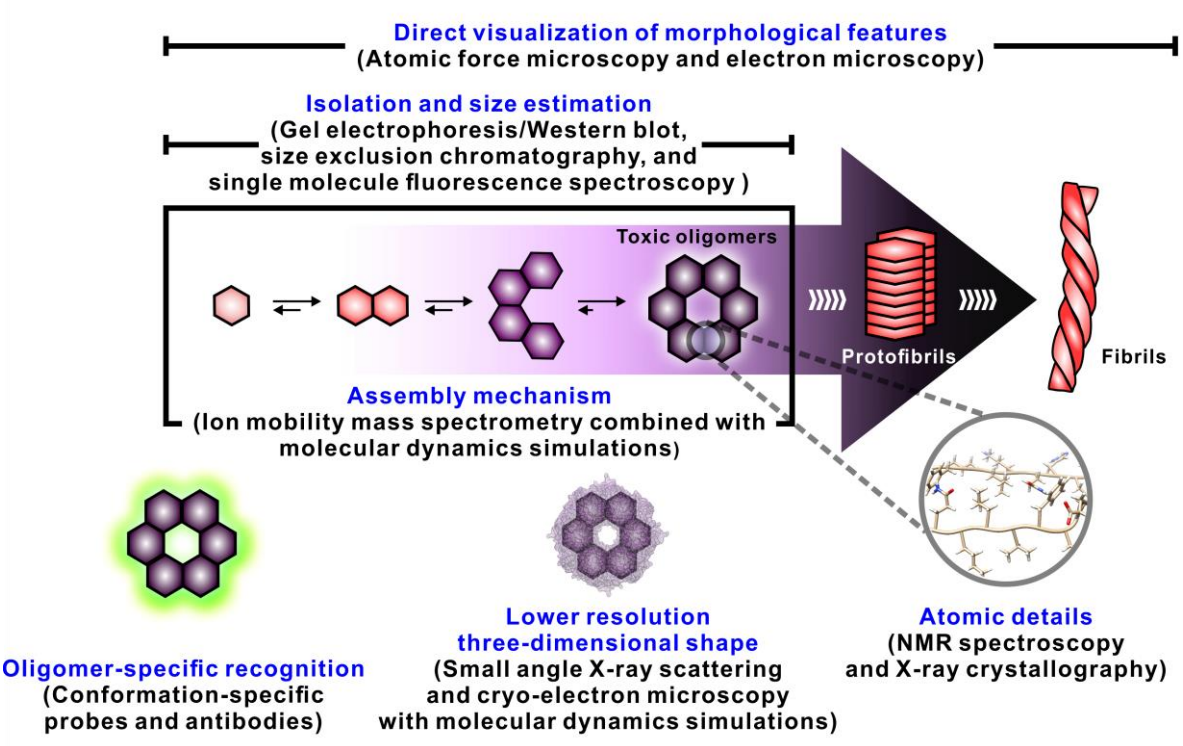

Figure 1.2. Methods to characterize Aβ oligomers. The isolation and size estimation of Aβ oligomeric species can be analyzed by gel electrophoresis, SEC, and single molecule fluorescence spectroscopy. Aβ aggregates and fibrils can be visualized by AFM and EM. Three-dimensional oligomeric conformations can be reconstructed by SAXS or cryo-EM in conjunction with MD simulations. Some probes and antibodies (*e.g.*, **BD-Oligo**, **A11**, and **KW1**) have been adopted to specifically target and recognize Aβ oligomers. More detailed structures at the atomic level can be supported by NMR spectroscopy and X-ray crystallography. The assembly mechanisms of Aβ oligomers are further identified by a combination of IM-MS and MD simulations, along with other methods described above.

1.3.1 Size Estimation of Toxic Aβ Oligomers

Although it has been suggested that toxic Aβ species possess specific multiple features, one challenge to the elucidation of a structure-toxicity relationship has been ambiguity over which species are responsible for toxicity. There have been a number of efforts towards this end to separate, isolate, and characterize oligomeric species from metastable heterogeneous mixtures, generally obtained from AD brain tissue or cultured AD cells.[9-11] The most widely employed techniques to separate and analyze the sizes of amyloid oligomers are polyacrylamide gel electrophoresis (PAGE)[8-12] and size exclusion chromatography (SEC).[9-11]

Ashe and coworkers used PAGE to isolate a 56 kDa Aβ species, probably dodecameric $Aβ_{42}$ based on its size in the gel, from brain extracts of 6-month-old AD transgenic mice with memory deficits.[9] The appearance of this 56 kDa Aβ species in immunoblots of mouse brain tissue coincided with onset of memory decline. Introduction of the isolated and purified 56 kDa Aβ directly into the lateral ventricle of healthy wild-type rats induced memory loss, assessed by a modified Morris water maze, a test of spatial learning and memory dependent on finding an invisible or visible platform that allows rats to escape the water. Thus, a causative link between the 56 kDa Aβ oligomeric species and memory deficits was affirmed.[9]

Based on separation by PAGE and SEC, Selkoe and coworkers demonstrated that Aβ trimers collected from 7PA2 cells expressing mutant human APP_{V717F} could deteriorate long-term potentiation (LTP) with greater potency than other oligomers in electrophysiological recordings on mouse hippocampal slices perfused with the purified trimers.[10] In a similar manner, dimers isolated directly from AD patients' brain samples by SEC had a comparable attenuating impact on LTP, and also affected memory when directly implanted into the brain of healthy wild-type rats.[11] LTP is a sustained increase in the strength of neuronal signals and the decline of LTP is associated with impaired signal transduction and deteriorated memory. These studies suggested that soluble diffusible Aβ oligomers as causative agents could diminish LTP and trigger some of the symptoms associated with AD.

PAGE and SEC are traditional but still widely used techniques. They are limited, however, in their ability to determine the exact size and precise distribution of oligomers. Single molecule fluorescence spectroscopy has been recently adopted to overcome the limited resolution of PAGE and SEC.[23] This method infers the number of Aβ monomers compromising an oligomeric assembly by counting the number of photobleaching steps of fluorophore-labeled Aβ peptides.[23] It is also sensitive and can be performed at low concentrations of Aβ closer to physiological levels, hence being more relevant to AD pathology. Since it is performed at the single molecule level, it also provides information on population heterogeneity rather than on an ensemble measurement. This is an important feature in the study of Aβ which adopts such diverse polymorphic states, and in a scenario where toxicity may arise from a minor Aβ species.

Recently, small angle X-ray scattering (SAXS) has been adopted to study Aβ oligomers' formation.[24] Although SAXS is a lower resolution method, it can examine shorter time scales of Aβ aggregation when combined with in-line rapid mixing to derive information on early events. In addition, computations from the scattering plot can reveal approximate oligomers' size (*i.e.*, diameter), molecular mass, and extent of polydispersity.[24] Ryan and coworkers employed SAXS to explore the influence of Cu(II) on $A\beta_{40}$ and $A\beta_{42}$ oligomerization in sub- and supra-stoichiometric amounts, motivated by the potential role of Cu(II) in AD pathogenesis.[7,24] They found that the less toxic $A\beta_{40}$ isoform was formed with elongated protofibril-like structures when Cu(II) was present, while $A\beta_{42}$ with supra-stoichiometric Cu(II) levels developed an ellipsoidal shape of $A\beta_{42}$ aggregates, closer to other reported toxic annular structures.[7,12,16,24,25] Thus, SAXS can be used to analyze Aβ oligomers' conformations generated in the early stage of aggregation.

1.3.2 Conformation and Topology of Aβ Oligomeric Species

Isolation of Aβ oligomers and determination of their size and distribution by PAGE and SEC pointed to the likely toxic species. To comprehend how the isolated oligomers could induce toxicity, analysis by additional methods is necessary to provide greater structural details with finer resolution because the morphologies of Aβ species are not just structural features, but correlated to their toxicity. Additionally, since amorphous oligomers generally lacking defined structures are typically regarded as nontoxic species,[14,26,27] whereas structured oligomers are indicated to be toxic,[12,16,17,25] it is necessary to reveal the particular structural attributes which trigger toxicity. Therefore, structural studies are absolutely critical to the study of Aβ oligomer-mediated pathogenesis, and a variety of techniques have been applied towards this goal.

The seminal ion mobility mass spectrometry (IM-MS) studies by Bowers *et al* detected various structures for $A\beta_{40}$ and $A\beta_{42}$ oligomers, and differences in their preferred configuration.[16,17] While $A\beta_{42}$ tetramers preferred a bent structure, they found that $A\beta_{40}$ tetramers adopted a distinct ring-shaped configuration. The ring-shaped $A\beta_{40}$ tetramers had a more enclosed configuration which could be less likely to form additional contacts; thus, the $A\beta_{40}$ tetramers tended to remain small species rather than grow into hexamers, dodecamers, or large aggregates.[16,17] Bent-shaped $A\beta_{42}$ tetramers had Aβ units at either end of the oligomer capable of forming additional contacts, and the IM-MS studies did in fact reveal that they could assemble further into larger donut-shaped dodecamers which had a seeding effect and accelerated protofibril elongation.[16,17] This study provided insight on the distinct toxicity profiles of the two isoforms, and demonstrated how the more toxic $A\beta_{42}$ could achieve this by forming dodecamers known to cause memory deficits.[16,17]

Actual structural topology can be obtained through imaging by atomic force microscopy (AFM) and electron microscopy (EM) that have been adopted to probe the morphologies of amyloid

oligomers and fibrils at the micrometer and nanometer scale.[7,12] An AFM study indicated that amyloid proteins, including Aβ peptides, were circularly arranged on lipid bilayers which constituted a membrane-permeable pore with a diameter of 8-12 nm.[12] The formation of such annular structures within cellular membranes could trigger influx into or efflux from cells leading to neuronal death and neurodegeneration, which provides an explanation for the toxic nature of structured Aβ oligomers compared to amorphous oligomers.[12,28]

Although structural details cannot be fully elucidated solely by AFM and EM, they can be complemented with other techniques, such as molecular dynamics (MD) simulations. For example, Nussinov and coworkers combined cryo-electron microscopy (cryo-EM) that illustrates three-dimensional architectural details at few nanometer scale, with MD simulations to reconstruct hollow tube assemblies or collapsed non-annular structures of $A\beta_{42}$ oligomers by matching simulated structures to the electron density map from cryo-EM.[25] The distinct polymorphs arose from whether the Aβ C-terminal faced outward (hollow tube) or inward (non-annular), the relative frequency of which was found to be pH dependent.[25] Neurotoxicity was associated with the hollow tube polymorph, yet it constituted the minor species at physiological pH according to the MD calculations. This suggests that toxic Aβ agents may not necessarily be the dominant form, making them critical to discern subpopulations of Aβ and emphasizing the complexity involved in full elucidation of all toxic forms.

1.3.3 Atomic Details of Aβ Oligomeric Species

The high-resolution structural analysis of Aβ oligomers has been challenging due to their inherent heterogeneity and metastability. One practical strategy to overcome this difficulty is to probe kinetically trapped oligomers at specific conditions; therefore, some atomic-scale structures of Aβ oligomers have been obtained by 2D NMR spectroscopy[20,21] and X-ray crystallography.[22] On the basis of peak width in 2D NMR, Ishii and coworkers reported that despite the size distribution in spherical prefibrillar $A\beta_{40}$ intermediates, they possessed some structural order with in-register parallel β-strand structure similar to fibrils. They were able to trap the transient intermediates formed upon incubation at 4 °C by freeze-trapping in liquid nitrogen, followed by 2D NMR collection at 15 °C.[20] Smith and coworkers identified structural properties of $A\beta_{42}$ pentamers stabilized at a low temperature (*ca.* 4 °C) and low salt concentration (*ca.* 10 mM).[21] These $A\beta_{42}$ pentamers were disordered, rather than β-stranded, but were relatively more toxic towards neurons than protofibrils or fibrils.[21] Nowick and coworkers elucidated the crystal structure of oligomers stabilized by incorporating a core $A\beta_{15\text{-}23}$ segment into macrocyclic β-strand peptides.[22] Although the macrocyclic peptides were artificially designed, their study demonstrated how the amyloid core sequence could generate various assemblies. For example, eight Aβ-incorporated cyclic peptides could align into a cruciform octamer which

further rearranged into larger oligomers, such as a triangular 24-mer and a hexagonal pore composed of three triangular dodecamers.[22] Complete atomic-level details on full-length Aβ oligomers at physiological conditions are still unavailable; however, the progress made in tackling such a challenging area has been remarkable and progresses forward. Such work continues to refine our understanding of a structure-toxicity relationship of Aβ oligomers.

1.3.4 Recognition of Aβ Oligomeric Species by Conformation-Specific Probes

Conformation-specific probes have been developed to recognize and detect the various forms of Aβ. Coupled to computational work, by the interaction of the probe with Aβ residues, the arrangement of hydrophobic residues relative to the surface of Aβ oligomers can be inferred. More importantly, these probes have enabled detection of the extracellular and intracellular localization of structured Aβ oligomers in tissues and in cells, which has contributed to our understanding of their toxicity (*vide infra*). An oligomer-specific small molecule fluorescent probe, BoDipy-Oligomer (**BD-Oligo**), was recently reported by Chang and coworkers based on a screen of a library of fluorescent compounds.[29] **BD-Oligo** was specific towards structured Aβ oligomers through π–π interactions of its aromatic rings with the exposed hydrophobic side chains of Aβ (*e.g.*, F19 and V36) as computational studies suggested.[29] Injections of **BD-Oligo** into APP transgenic AD mice demonstrated its low toxicity, blood-brain barrier (BBB) permeability, and potential as an *in vivo* imaging agent showing that it could be co-localized with Aβ plaques in brain sections.[29]

In addition to synthetic molecules, there are some antibodies that specifically recognize Aβ oligomers, the most widely used of which is **A11**, first introduced by Glabe and coworkers.[30] **A11** recognizes soluble amyloid oligomers (*e.g.*, Aβ, islet amyloid polypeptide (IAPP), and α-synuclein oligomers) demonstrating the universal conformational properties of toxic structured oligomers.[30] Recently, Fändrich and coworkers reported another oligomer-specific antibody, **KW1**, which could selectively target Aβ oligomers with antiparallel β-sheet even in homogenates of AD brain tissue.[31] The selectivity of **KW1** originates from interactions with surface-exposed hydrophobic motifs in oligomeric species which are buried in fibrils.[31] Although it is hard to obtain atomic details of amyloid oligomers by using oligomer-specific probes, interactions between Aβ oligomers and these probes provide clues to the relative arrangement of hydrophobic or aromatic residues.[31] Despite their limited use for structural determination, these probes have been invaluable to the elucidation *in vivo* of Aβ oligomers' location. In addition, the antibodies have found practical applications in biochemical and cell molecular techniques, such as Western blot and immunoprecipitation, in the study of mechanisms of toxicity of Aβ oligomers. Even with the inherent challenges to elucidating structural details on transient, metastable species, progress has been made by collating results from multiple techniques at various levels of resolution (Figure 1.2) to assess numerous structural aspects of Aβ, gaining a

comprehensive perspective. Equipped with these insights into structural characteristics of Aβ oligomers, the monumental but critical task of correlating structures with neurotoxicity is also underway, as described in the following section.

1.4. Mechanisms of Toxicity Induced by Aβ Oligomers

It is becoming increasingly evident that soluble, diffusible Aβ oligomers manifest neurotoxicity in AD. Due to the heterogeneous environment and properties in living organisms and of Aβ oligomers themselves, the mechanisms by which Aβ oligomers can prompt toxic effects on cellular systems and activate neuronal death are complex and challenging to comprehend. In spite of the obstacles, investigations with multiple methods have presented greater information about Aβ oligomers' toxicity towards intracellular and extracellular systems, which we discuss in this section on the basis of recent findings (Figure 1.3).

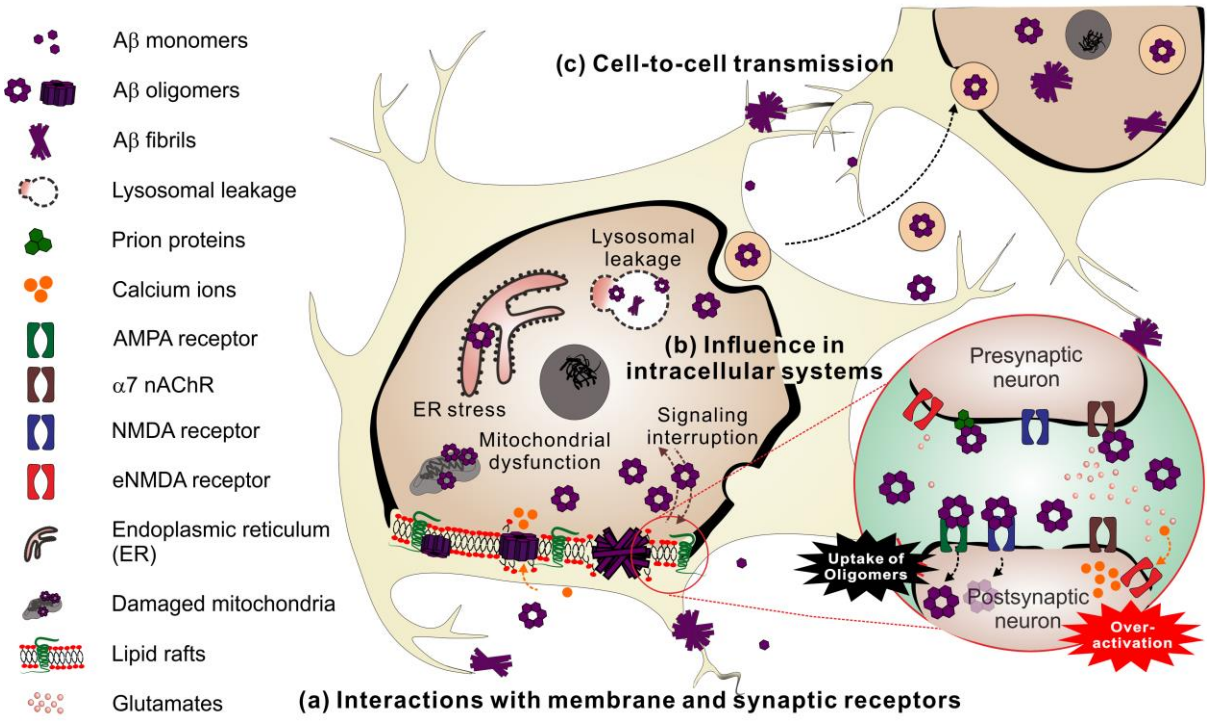

Figure 1.3. Proposed mechanisms for toxicity triggered by Aβ oligomers. (a) Interactions of Aβ oligomers with lipid rafts in membrane and membrane-bound synaptic receptors can disrupt membrane microenvironments. (b) Aβ oligomers can be internalized *via* association with synaptic receptors and accumulate in subcellular compartments, causing damage to organelles and signaling pathways. (c) Cell-to-cell transmissible properties of Aβ oligomers could contribute to the propagation of neuropathology.

1.4.1. Interactions of Aβ Oligomers with Membranes and Membrane Receptors

Extracellular Aβ oligomers can affect membranes on multiple levels. They can (i) bind to the

membrane causing local perturbations that damage it;[28,32,33] (ii) bind to receptors on the membrane that influence signal transduction,[34,35] induce endocytosis of oligomers into the cell,[34,36] or trigger damage due to aberrant cellular signaling;[35] (iii) form annular structures that insert into the membrane leading to unregulated efflux/influx through the created pores (Figure 1.3).[28,37] Multiple studies have undergone to address these various modes of Aβ oligomers' toxicity in great detail, too numerous to comprehensively review herein. Therefore, we highlight a few on each mechanism in turn, in order to illustrate key features of Aβ oligomers' interactions with cellular membranes.

Both *in vivo* and *in vitro* studies have proposed an interplay between Aβ oligomers and lipid rafts which are membrane domains mainly consisting of cholesterol, GM1-ganglioside sphingolipids, and synaptic receptors.[28,32,33] Aβ dimers were found to accumulate at lipid rafts in the brains of a transgenic Tg2576 mouse model which overexpresses Swedish mutant human APP.[32] Although the net Aβ concentration *in vivo* is below the threshold that initiates aggregation *in vitro*, this dense accumulation at lipid rafts could raise the local Aβ concentration and thus seed Aβ aggregation and plaque formation.[32] Another technique, isothermal titration calorimetry adopted by Selkoe and coworkers, reaffirmed the observation that Aβ oligomers could interact with lipid membranes more rapidly than monomers.[33] An immunoprecipitation assay indicated that Aβ dimers were associated with GM1-gangliosides in lipid rafts.[33] Since lipid rafts are centers of signal transduction, the dense collection of Aβ oligomers at those sites could interfere with signal transduction, which could lead to memory decline. This possibility is supported by the correlation of Aβ dimers' accumulation at lipid rafts in 6-months old Tg2576 mice with onset of memory impairment.[32] Furthermore, fibrillization of Aβ oligomers that are concentrated at membranes and lipid rafts can cause membrane fragmentation and damage, aggravating Aβ-triggered toxicity.[28]

Other factors contributing to cognitive deterioration in AD are the attenuation of LTP, lowered synaptic plasticity, and decline of spine density, all of which give rise to synapse loss (Figure 1. 3a).[34,35] Although these neuropathological features of AD have been known for some time, recent studies have been bringing mechanistic details to light. They have been revealing that the interaction of Aβ oligomers with membrane receptors could be one prominent factor in the initiation of synapse loss.[34,35] In one study, treatment of human and rat astrocytes with Aβ oligomers increased glutamate release as measured by a FRET-based glutamate sensor system (FRET, Förster resonance energy transfer), which was not observed following treatment with Aβ monomers.[34] Glutamate release was found to be calcium dependent, and thus a calcium permeable receptor was sought to mediate this effect. It was discovered that glutamate release was initiated by binding of human-derived Aβ trimers to astrocytic α7 nicotinic acetylcholine receptors (α7 nAChR), a calcium permeable ion channel.[34] The excessive discharge of glutamate overactivated extrasynaptic *N*-methyl-D-aspartate receptors (eNMDARs) on hippocampal neurons decreasing synaptic currents.[34]

In addition to aberrant release of neurotransmitters, complexation of Aβ oligomers with receptors (*e.g.*, NMDAR, α-amino-3-hydroxy-5-methyl-4-isoxazolepropionate (AMPA) receptor, and α7 nAChR) also promoted internalization of oligomers through endocytic pathways which triggered damage to intracellular systems (*vide infra*).[36] The interaction may also alter signaling pathways downstream of receptor binding. For example, inappropriate activation of eNMDARs increased calcium influx into neurons, initiating the activity of nitric oxide (NO) synthase able to raise the concentration of NO, which could lead to apoptosis.[34] Elevated NO levels could also lead to enhanced nitrosylation of cyclin-dependent kinase 5 (Cdk5), in turn causing S-nitrosylation of dynamin-related protein 1 (Drp1), correlated with synaptic spine loss.[34] Dendritic spines are small protrusions from neuron dendrites that generate synapses with axons from other neurons. Therefore, a loss of spine density results in degeneration of neuron synapses and connectivity.

There are other signaling pathways that affect synaptic spine density. Cellular prion protein (PrP^c) is abundant in postsynaptic densities and binds to Aβ oligomers.[35] Complexes of PrP^c with Aβ oligomers activate the kinase Fyn which has the dual effect of decreasing NMDAR density at the synapse and causing dendritic spine loss.[35] Thus, the activation of Fyn exacerbates Aβ oligomers' toxicity since both receptor and spine density are diminished at synapses.

Along with interactions with membranes and receptors and concomitant aberrant signaling, Aβ oligomers can also perforate membranes.[28,37] The antiparallel β-sheet conformation of Aβ oligomers has structural similarities to porin, a β-barrel-like bacterial outer-membrane protein.[37] Porin can disrupt cellular systems by penetrating into membranes, leaving channels large enough to allow passive diffusion of smaller-sized molecules thus dysregulating the cellular environment.[37] Several studies have shown that in a similar manner, pore-shaped structured Aβ oligomers can cause membrane leakage by penetrating membranes.[12,28,37] This was demonstrated by a dye leakage assay in ganglioside-rich large unilamellar vesicles which were used as a model for lipid rafts.[28] Dye leakage was observed from the vesicles within minutes following treatment with Aβ.[28] The leakage could be blocked by treatment with Zn(II), indicating that cation-selective channels were formed upon Aβ treatment, presumably by the insertion of annular Aβ oligomers into the vesicle membrane.[28] Dye leakage continued following prolonged exposure to Aβ with onset of fibrillization, except this dye leakage was no longer receptive to Zn(II). It indicated that leakage occurred from mechanically fragmented membranes, not pores.[28] This suggests that early damage to membranes by Aβ is intiated by pore formation, and the membrane breaks up mechanically when fibrillization occurs. This damage could enhance the uptake of calcium ions, leading to calcium dyshomeostasis, a major aspect of AD pathology and dysregulation of which leads to impaired signal transduction and aggravated cellular degeneration.[12,28,34] When gangliosides were omitted from the vesicles, leakage was much less pronounced, confirming other experiments that Aβ oligomers bind to GM1-ganglioside.[33]

Overall, recent studies suggest that Aβ oligomers can induce toxicity by interacting directly with cellular membranes and with membrane receptors that activate various signaling pathways. Annular Aβ structures can perforate the membrane leading to additional dysregulation of neurons, and fibrillization at the membrane can mechanically disrupt it. Further investigation of these mechanisms will bring greater clarity on Aβ oligomers' mechanisms of toxicity which can potentially reveal therapeutic targets if the pathways can be blocked. This line of thought has already been tested.[34,35]

1.4.2 Influence of Aβ Oligomers on Intracellular Processes

Aβ monomers are secreted into the extracellular space when they are cleaved off from APP.[2] This extracellular Aβ pool can interact with membranes and receptors, and can also be internalized into neurons by endocytic vesicles. Additionally, Aβ can accumulate intracellularly by the production of Aβ peptides at organellar membranes where a portion of APP is localized.[38-40] Numerous organelles are implicated as sites for Aβ generation and aggregation, such as mitochondria, trans-Golgi network, endoplasmic reticulum (ER), endosomes, autophagosomes, and lysosomes.[38-40] The presence of intracellular Aβ oligomers within organelles and at organellar membranes can provoke (Figure 1.3b) (i) elevated ER stress, (ii) calcium ion dyshomeostasis, (iii) mitochondrial damage, (iv) altered proteolysis, and (v) apoptosis. All these events of cellular damage caused by Aβ oligomers can initiate cell death.[38-40]

Mori and coworkers employed $APP_{E693\Delta}$ transgenic mice which express a mutant Aβ that oligomerizes but does not fibrillize.[38] Although this mutation does not affect Aβ production, it can increase the level of intracellular Aβ species. Immunohistochemistry of brain sections from $APP_{E693\Delta}$ transgenic mice demonstrated that Aβ oligomers were co-localized with cellular organelles (*i.e.*, ER, endosomes, lysosomes, and mitochondria) in neurons.[38] Moreover, compared with wild-type or APPwt-transgenic mice, $APP_{E693\Delta}$-transgenic mice exhibited elevated levels of Grp78 (a molecular chaperone) and HRD1 (an E3 ubiquitin ligase which tags unfolded molecules for removal and destruction). Both are markers indicative of elevated ER stress in $APP_{E693\Delta}$-transgenic mice, which was attributed to the intracellular accumulation of Aβ oligomers.[38] Aβ oligomers can also trigger ER stress through calcium dyshomeostasis.[39] In cultured primary cortical neurons, Pereira and coworkers suggested that Aβ oligomers induced calcium dyshomeostasis in ER by activation of phospholipase C signaling, which can initiate release of calcium from the ER to the cytosol.[39] In addition, the Aβ oligomer-mediated calcium dyshomeostasis led to decreased cell viability and activation of caspase 3, an enzyme that represents the apoptotic pathway.[39]

Oligomeric Aβ can also trigger mitochondrial malfunction,[38,40] which is thought to be linked to synaptic dysfunction and memory impairment.[40] Aβ oligomers abnormally depolarize mitochondrial

membranes, releasing cytochrome c, which signals apoptosis when detected in the cytosol.[38] Mitochondrial fragmentation from excessive fission provoked by Aβ oligomers has been considered as an additional factor of mitochondrial dysfunction.[40] Aβ oligomer-activated S-nitrosylation of dynamin-related protein 1 (Drp1), the protein responsible for mitochondrial fission, was proposed by Lipton and coworkers as a route to mitochondrial dysfunction.[40] Elevated levels of S-nitrosylated Drp1 were in fact found in the brains of human AD patients and Tg2576 transgenic mice, validating the hypothesis and suggesting that Aβ oligomers could damage the energy producing capabilities of neurons leading to further degradation in neuronal function.[40] Lastly, proteolysis and intracellular signaling are also perturbed by Aβ oligomers.[38,41] Aβ oligomers cause lysosomal and endosomal membrane leakage, impair proteolysis, and increase efflux of lysosomal enzymes to the cytosol, thereby leading to apoptosis.[38] Dispersion of lysosome-specific cathepsin D enzyme into the cytosol of $APP_{E693\Delta}$-transfected cells implied that lysosomal and endosomal membranes had been ruptured.[38] By damaging endosomal vesicles, Aβ oligomers can interfere with retrograde transport (from synapse towards nucleus) of BDNF (brain-derived neurotrophic factor) vesicles, a signaling pathway essential to synaptic plasticity and memory.[41] Aβ oligomers could downregulate ubiquitin C-terminal hydrolase L1, a deubiquitinating enzyme, interfering with proteolysis and possibly resulting in signal disruption.[41]

1.4.3 Transmission of Aβ Oligomers

The ability of Aβ to seed plaque formation and spread in the brain has been demonstrated in mouse and primate models, and has been likened to prion disease.[13,42] This transmissible characteristic of Aβ has recently been confirmed in human autopsies of patients who had received human cadaver-derived growth hormone to treat short stature. Along with the detection of prion Creutzfeldt–Jakob disease (CJD), moderate to severe deposition of Aβ plaques which did not co-localize with prion was also observed.[13] These patients were aged 36-51 and did not harbor any genetic mutations that were commonly associated with early onset familial (inheritable) AD. The suspicion was that AD pathology could have arisen from growth hormone preparations that were inadvertently contaminated with Aβ in addition to prion, suggesting Aβ-associated pathology may also be transmissible in humans.[13] Although the study did not involve a very large number of autopsies (n = 4), the results merit consideration and further study.

The spread of Aβ in the brain may occur through a seeding effect of extracellular Aβ in the spaces between neurons. It may also occur from intracellular accumulation from endocytosis of Aβ or intracellularly processed APP at organellar membranes. Some investigations, however, have suggested that Aβ oligomeric seeds could even spread to distant regions *via* a cell-to-cell transmission mechanism (Figure 1.3c).[42] Employing a system of donor (contains Aβ) and acceptor (receives Aβ)

neurons embedded in a 3D configuration, where the fluorescently labeled Aβ could be tracked from donor to acceptor, Nath and coworkers found that several Aβ isoforms transferred ($Aβ_{40}$, $Aβ_{42}$, and $Aβ_{3pE-40}$) to varying degrees with $Aβ_{42}$ expressing the highest level of transmissibility.[42] The accumulation of Aβ within endosomes and the control of Aβ's transfer with inhibitors of endosome formation suggested that the cell-to-cell transfer of oligomeric Aβ isoforms was mediated by the endosomal trafficking system.[42] Continuous cell-to-cell propagation of oligomers resulted in large lysosomal vesicles which could dysregulate lysosomes in both donor cells and acceptor cells.[42] This transmissible property of Aβ oligomers could be one molecular mechanism by which Aβ pathology may expand in the brain,[13,42] but many more studies are required to construct a comprehensive view.

1.5. Inhibitors against Aβ Aggregation

Since the evidence against Aβ oligomers as toxic agents has mounted, some chemical agents have been devised to specifically modulate them or control the aggregation pathways that lead to their accumulation.[14,15,26,27,43-51] Design approaches for such agents have focused mainly on (i) inhibition of Aβ oligomerization;[14,43,44] (ii) disaggregation of preformed Aβ oligomers;[15] (iii) suppression of toxic aggregate formation by redirection of on-pathway aggregates into nontoxic off-pathway aggregates;[14,26,27,45,46] (iv) disruption of secondary nucleation which otherwise accelerates the growth of toxic Aβ oligomers.[47]

One method to develop chemical agents for biological applications is to screen chemical libraries, composed of known compounds, for potential biological activity.[14,15,26,43] Several natural products and synthetic molecules that attenuate Aβ oligomer-associated toxicity have been discovered in this manner.[14,15,26,43] Another approach to expand beyond existing agents and obtain more effective chemical tools is to derivatize the molecules found through screening or to newly design and synthesize compounds.[46,48,49] Recently, rational design of such chemical agents that regulate Aβ oligomers and other AD pathogenic aspects (*e.g.*, metals, reactive oxygen species (ROS)) has been successful *via* a (i) linkage[48] or (ii) incorporation[46,49] approach. In the linkage approach, two or more moieties known to interact with Aβ oligomers and/or fibrils are combined together by a chemical linker.[48] In the incorporation strategy, the structural portions for interactions with Aβ and other pathogenic agents are incorporated into the same molecular framework, affording a compact molecule.[46,49] Moreover, along with small synthetic molecules and natural products, short peptides, protein domains, and oligomer-specific antibodies have also been utilized to inhibit the production of Aβ oligomers or redirect their aggregation.[44,47,50] In this section, we describe the recent progress in the development of some chemical agents against Aβ aggregation, including oligomerization, in order to diminish their toxicity.

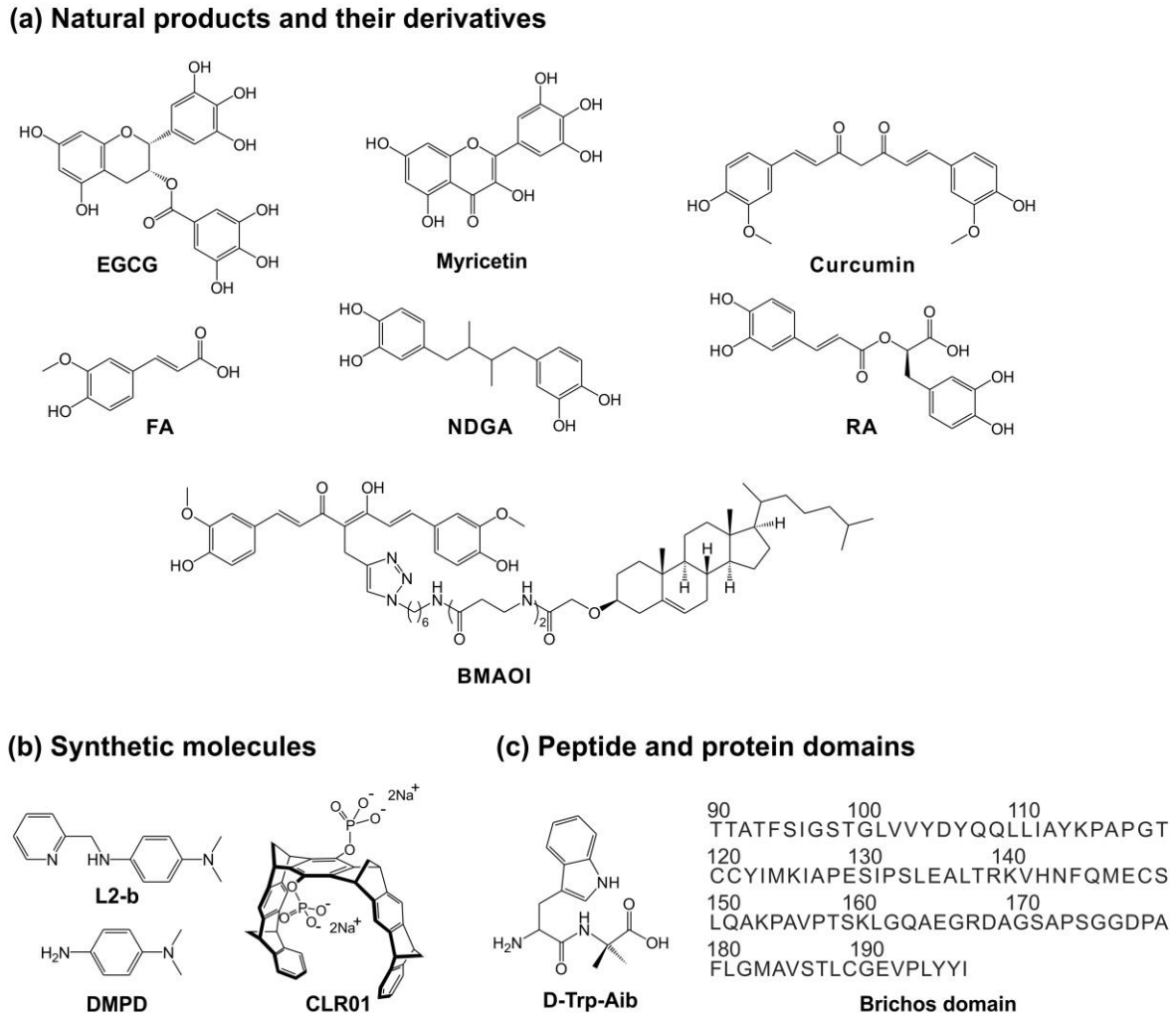

Figure 1.4. Selected chemical agents to control Aβ aggregation, including oligomerization. Chemical structures of (a) natural products and their derivatives; (b) synthetic molecules; (c) peptide and protein domains.

1.5.1. Natural Products and Their Derivatives

Epidemiological studies have indicated that dietary factors might impact the incidence of AD and therefore natural products have garnered interest as possible modulators of Aβ. Various natural products have been found to exert a significant influence on Aβ aggregation thereby diminishing the toxicity from Aβ oligomers (Figure 1.4a).[14,15,26,43,51] Therefore, researchers have directed their efforts towards the elucidation of mechanisms by which natural products might redirect Aβ aggregation pathways.[14,15,26,43,51] Tessier and coworkers categorized natural polyphenols by their ability to attenuate Aβ oligomers' formation *via* (i) remodeling Aβ oligomers into nontoxic and/or unstructured aggregates; (ii) converting oligomers into relatively inert fibrils; or (iii) disassembling structured

oligomers into low molecular weight species (*i.e*. nontoxic monomers).[15] Utilizing immunoblotting and microscopic methods (*i.e*., AFM and TEM), they found that naturally occurring polyphenols altered Aβ aggregation pathways presumably by interfering with π–π stacking between aromatic Aβ residues and producing covalent adducts with Lys residues in Aβ peptides.[15,51]

One naturally occurring abundant polyphenolic compound found in green tea extracts, (−)-epigallocatechin gallate (**EGCG**; Figure 1.4a), was shown to inhibit on-pathway Aβ oligomerization and fibrillization as well as disaggregate preformed aggregates, which was indicated to promote the formation of nontoxic amorphous Aβ oligomers.[14,26] Interaction of **EGCG** with the N-terminal and central helical regions of Aβ was revealed by 2D NMR spectroscopy, indicating how **EGCG** might affect Aβ oligomerization.[14,26] In addition, **EGCG**'s reactivity with Aβ was enhanced in the presence of metal ions *in vitro*, which is another benefit since metal ion dyshomeostasis plays a role in AD pathogenesis.[26] Compaction of Aβ by **EGCG** in both the absence and presence of metal ions was observed by IM-MS with MD simulations, suggesting that **EGCG** could alter Aβ oligomers' conformations.[26] Moreover, **EGCG** was observed to reduce toxicity triggered by both metal-free and metal-associated Aβ in cultured cells.[14,26]

Myricetin, **curcumin**, nordihydroguaiaretic acid (**NDGA**), rosmarinic acid (**RA**), and ferulic acid (**FA**) (Figure 1.4a) are natural products that may also be capable of blocking oligomerization.[43] PAGE gels with silver staining showed a dose-dependent inhibitory function of these natural products towards $A\beta_{40}$ and $A\beta_{42}$ aggregation showing fewer oligomer formation.[43] NMR studies indicated that **NDGA** and **FA** bound to specific amino acid regions of Aβ (*e.g*., Arg5, Ser8, Gly9, His13, Lys16, Asp23, and Ile31) while **myricetin** caused shifts in the majority of Aβ residues, implying a more global conformational change.[43] When $A\beta_{40}$ and $A\beta_{42}$ were incubated with these natural polyphenols, they were stabilized in a random coil state which inhibited conversion to β-sheets.[43] LTP and long-term depression (LTD) assays on hippocampal slices presented that synaptotoxic effects induced by Aβ oligomers were impeded in the presence of **myricetin** and **RA**.[43]

Natural products can be utilized to produce new chemical tools that modulate Aβ aggregation by rational design and structural modifications.[48] For instance, Aβ peptides bind to components in lipid rafts (*e.g*., cholesterol and sphingolipids) and their oligomerization can be prevented by polyphenols.[48] Zhang and coworkers adopted a rational modification stratagem by taking advantage of the ability of two natural products (*i.e.*, cholesterol for binding Aβ and curcumin for inhibiting aggregation).[48] Following the linkage approach, they conjugated cholesterol with curcumin to design bivalent multifunctional Aβ oligomerization inhibitors (**BMAOI**s; Figure 1.4a).[48] The inhibitory effect of **BMAOI** on Aβ oligomerization or aggregation in ML60 cells was dependent on the linker length.[48] Co-localization of **BMAOI** with Aβ oligomers and membranes in MC65 cells was observed

by immunocytochemistry, confirming that **BMAOI** could interact with Aβ oligomers as well as be localized to membranes and lipids where Aβ oligomers could accumulate.[48] **BMAOI**′s protective effect and antioxidant ability were also observed.[48]

1.5.2 Synthetic Molecules

Synthetic compounds have been rationally designed to interact with Aβ peptides and modulate their aggregation pathways.[45,46,49] As an example, a small molecule, **L2-b** (Figure 1.4b), was observed to control metal-bound Aβ complexes (metal–Aβ; *e.g.*, Cu(II)–Aβ and Zn(II)–Aβ) through generation and stabilization of Aβ species into unstructured, nontoxic oligomeric species.[46,49] **L2-b** was constructed by the incorporation approach in which metal chelation sites (two nitrogen donor atoms) were directly installed into the stilbene framework, known to interact with Aβ peptides.[46,49] **L2-b** noticeably modulated metal–Aβ aggregation over metal-free Aβ aggregation *in vitro* as intended by the design strategy. IM-MS and NMR studies indicated **L2-b**'s efficacy in modulating the activity of metal–Aβ species *via* its formation of a ternary complex with metal–Aβ complexes.[46,49] Additionally, in the case of Cu(II)–Aβ, **L2-b** could further trigger peptide fragmentation through transient ternary complexation with Cu(II)–Aβ.[46] *In vivo* efficacy testing of **L2-b** in 5xFAD AD mice demonstrated that this molecule could diminish the amount of Aβ species in the brain and improved learning and memory abilities.[46]

Lim and coworkers have recently reported a compact and redox-active molecule, *N*,*N*-dimethyl-*p*-phenylenediamine (**DMPD**; Figure 1.4b), which contains moieties (*i.e.*, dimethylamino group and one nitrogen donor atom) that potentially interact with metal-free Aβ, metal–Aβ, and metal ions.[27] **DMPD** was indeed found to effectively regulate the aggregation of both metal-free and metal-associated Aβ peptides.[27] In contrast to noncovalent aggregation inhibitors, the noticeable activity of **DMPD** towards metal-free Aβ and metal–Aβ was achieved *via* covalent crosslinking between primary amine-containing residues (*e.g.*, Lys16 in Aβ) and the transformed **DMPD** (*i.e.*, *p*-benzoquinone), as confirmed by MS.[27] IM-MS presented that the adduct between transformed **DMPD** and Aβ adopted a more compact conformation than compound-untreated Aβ, producing unstructured amorphous forms. Additionally, the potential interactions of **DMPD** with hydrophobic residues in the self-recognition and C-terminal regions of Aβ were implicated by a combination of 2D NMR spectroscopy and MD simulations.[27] Treatment of 5xFAD AD mice with **DMPD** led to decreased loads of toxic amyloid oligomers in the brain with concomitant improvement in cognitive function.[27]

Some inhibitory agents exert their effect by generating nontoxic amyloid species *via* off-pathway oligomerization rather than by simply decelerating fibrillation kinetics. Synthetic small molecules (*e.g.*, **L2-b** and **DMPD**) can redirect Aβ peptides into such amorphous nontoxic Aβ

oligomers.[27,46] In particular, **L2-b** could produce nontoxic amorphous Aβ oligomers specifically in the presence of Cu(II) and Zn(II).[46] Therefore, since these small molecules can induce relatively nontoxic oligomers, they can lower toxicity linked to Aβ oligomers in cultured cells and/or *in vivo*.[27,46]

A synthetic molecular tweezers, **CLR01** (Figure 1.4b), exhibited reactivity against amyloid aggregation by inhibiting oligomerization and fibrillization, and by the disassembly of preformed aggregates.[45] **CLR01** binds specifically to Lys residues by virtue of electrostatic interactions between its phosphate groups and the ammonium group of Lys, in addition to hydrophobic interactions between the aromatic sides of **CLR01** and the lysine butylene moiety.[45] Therefore, **CLR01** grips Lys residues like a pair of tweezers, with an affinity great enough to disrupt unfolded, Lys-containing proteins, but not interfere with well-folded, non-amyloidogenic proteins. The premise for the design of **CLR01** was confirmed by a thioflavin-T (ThT) fluorescence assay (quantification of fibril formation) and dot blot assay (immunoblot for the amount of oligomeric Aβ) which exhibited that **CLR01** inhibited Aβ aggregation, including oligomerization. NMR analysis suggested that **CLR01** could affect amyloid aggregation by interacting with Lys residues of $A\beta_{42}$ (*i.e.*, Lys16 and Lys28).[45] MD simulations indicated that the intermolecular interactions between two $A\beta_{42}$ monomers could be hindered by **CLR01** binding to Lys residues of $A\beta_{42}$.[45]

1.5.3 Peptides or Protein Domains

A small dipeptide, D-tryptophan linked with α-aminoisobutyric acid (**D-Trp-Aib**; Figure 1.4c), was prepared to target amyloid oligomers that form in the early stage of Aβ aggregation.[44] **D-Trp-Aib** was selected from a library composed of 40 inhibitors to satisfy several criteria: (i) containing a β-breaker motif that is a moiety capable of disrupting β-sheets; (ii) having an "aromatic binder" to interact with hydrophobic residues in Aβ; (iii) being metabolically stable D-amino acids for biomedical purposes.[44] In the lead candidate, **D-Trp-Aib**, the **Aib** portion is the potent β-breaker, while the tryptophan is composed of an aromatic indole group for Aβ binding. Additionally, as expected, based on its D-amino acid constitution, **D-Trp-Aib** was stable in serum for 24 h, and possessed other attributes including low toxicity and some BBB permeability.[44] Analyses by gel electrophoresis and EM demonstrated that **D-Trp-Aib** reduced the generation of low molecular weight oligomers *in vitro*.[44] NMR investigations suggested that the inhibitory activity of **D-Trp-Aib** against Aβ oligomers could be linked to its interactions with the aromatic rings of Phe19 and Phe20, the residues located in the self-recognition site of Aβ (Leu17-Ala21).[44] Moreover, administration of **D-Trp-Aib** to AD transgenic mice diminished amyloid plaques in brain tissue concomitant with cognitive improvement.[44]

Recently, modified antibodies have been adopted to inhibit the formation of amyloid aggregates (Figure 1.4c).[50] Tessier and coworkers designed Grafted AMyloid-Motif AntiBODIES, abbreviated

gammabodies, by fusing either $A\beta_{18-21}$ (part of the self-recognition motif) or $A\beta_{33-42}$ (C-terminal) peptide fragments to a single domain antibody.[50] The resultant **gammabodies** bound Aβ oligomers (grafted $A\beta_{33-42}$) and fibrils (grafted $A\beta_{18-21}$ and $A\beta_{33-42}$) with nanomolar affinity. They could redirect Aβ aggregation pathways by forming small gammabody–Aβ complexes and were so potent that they could still stabilize Aβ monomers as unstructured conformers even after 6 day incubation.[50] This inhibitory effect of **gammabodies** was achieved at sub-stoichiometric concentrations, a feat not achieved by conventional antibodies which sequester Aβ in near stoichiometric amounts. Some previously reported conformation-specific antibodies were effective at sub-stoichiometric levels, but did not achieve it in a manner similar to **gammabodies** which sequestered Aβ as small nontoxic clusters.[50]

Another example of protein-based inhibitors is **Brichos** (Figure 1.4c), an approximately 100 amino acid domain from the prosurfactant protein C precursor (proSP-C), a member of the **Brichos** family of proteins.[47] The **Brichos** domain of proSP-C possesses chaperone-like activity.[47] A series of Aβ aggregation experiments were conducted in the absence and presence of **Brichos**, going to great lengths to ensure reproducibility in the aggregation kinetics by careful control of subtle experimental parameters. By using modeling to predict the kinetics of fibril formation if **Brichos** inhibited one of three principal steps (*i.e*. primary nucleation, fibril elongation, and secondary nucleation), they found that the best fit between experiment and prediction occurred if **Brichos** prevented secondary nucleation.[47] **Brichos** was able to achieve this remarkable control of secondary nucleation by binding directly to Aβ fibrils. Furthermore, the total level of monomers and oligomers was measured with and without **Brichos** presenting that **Brichos** significantly lowered the amount of toxic oligomers, presumably by controlling secondary nucleation, the primary source of oligomers at physiological concentrations of fibrils.[18,47] Concomitant with the control of toxic Aβ oligomers' formation, **Brichos** could also reduce signal impairment in $A\beta_{42}$-treated hippocampal brain slices from C57BL/6 mice.[47]

1.6. Conclusion

AD is considered an amyloidogenic disorder characterized by the accumulation and aggregation of misfolded Aβ peptides. During aggregation, polymorphic species are generated from Aβ monomers yielding a heterogeneous population of transient on-pathway Aβ oligomers that are eventually transformed to larger protofibrils and fibrils. The structured Aβ oligomeric intermediates are suggested to be the primary toxic agents while fibrils are indicated to be inert and relatively less toxic, but can still act as a reservoir of toxic oligomers by fragmentation and secondary nucleation. Recent advancements in biochemical and biophysical methods have revealed some structural characteristics of Aβ oligomers: (i) isolation and size estimation of oligomeric species have been achieved by PAGE, SEC, and single molecule fluorescence spectroscopy; (ii) knowledge of assembly pathways of

multiple oligomeric intermediates at the molecular level have been obtained by IM-MS combined with MD simulations; (iii) morphological and topological features have been directly visualized by AFM, EM, single molecule fluorescence spectroscopy, and SAXS; (iv) atomic details of Aβ oligomers have been provided by NMR spectroscopy and X-ray crystallography; (v) recognition and targeting of oligomeric species are enabled by conformation-specific probes and antibodies.

Along with advances in Aβ oligomers' characterization, several toxicity mechanisms mediated by structured Aβ oligomers have also been proposed. Aβ oligomeric species can exert toxic effects through extracellular interactions with membranes or membrane-bound receptors, accumulation at intracellular organelles, and cell-to-cell transmission. Until now, a clear relationship between oligomers' structural properties and toxicity has not been fully established; however, the involvement of Aβ oligomers in AD pathogenesis has been recognized. This has initiated a search for strategies to manage Aβ oligomers to alleviate toxicity. Several natural products, synthetic molecules, and protein domains have been discovered or designed to modulate Aβ aggregation as a therapeutic strategy. Some inhibitory agents lowered the amount of amyloid oligomers in the brain and improved cognitive deficits in animal AD models, suggesting their potential to be utilized for designing new drug candidates.

Despite the recent progress in elucidating a structure-toxicity relationship of Aβ oligomers and the development of inhibitors against Aβ aggregation, multiple important questions remain unanswered. The conformations of some Aβ oligomers have been elucidated; however, it is unclear whether oligomeric species with different structures have distinct biological roles, and which oligomeric state is the most pathologically-relevant form. In addition, it is still obscure how the conformations of oligomeric species and their interactions with cellular organelles (*e.g.*, lysosomes, mitochondria, and ER) can be correlated with toxicity. Overall, the identification of such fundamental aspects will be crucial to gain mechanistic insights into AD pathogenesis as well as advance the discovery of novel diagnostics and therapeutics.

1.7. Acknowledgments

Research in the Lim Lab is currently supported by the National Research Foundation (NRF) of Korea which is funded by the government of Korea (NRF-2014S1A2A2028270; NRF-2014R1A2A2A01004877; NRF-2016R1A5A1009405) and the 2016 Research Fund (Project Number 1.160001.01) from Ulsan National Institute of Science and Technology (UNIST).

1.8. References

1. F. Chiti and C. M. Dobson, *Annu. Rev. Biochem.*, 2006, **75**, 333-366.
2. J. A. Hardy and G. A. Higgins, *Science*, 1992, **256**, 184-185.

3. R. D. Terry, E. Masliah, D. P. Salmon, N. Butters, R. DeTeresa, R. Hill, L. A. Hansen and R. Katzman, *Ann. Neurol.*, 1991, **30**, 572-580.
4. W. L. Klein, G. A. Krafft and C. E. Finch, *Trends Neurosci.*, 2001, **24**, 219-224.
5. M. P. Lambert, A. K. Barlow, B. A. Chromy, C. Edwards, R. Freed, M. Liosatos, T. E. Morgan, I. Rozovsky, B. Trommer, K. L. Viola, P. Wals, C. Zhang, C. E. Finch, G. A. Krafft and W. L. Klein, *Proc. Natl. Acad. Sci. USA*, 1998, **95**, 6448-6453.
6. A. Y. Hsia, E. Masliah, L. McConlogue, G.-Q. Yu, G. Tatsuno, K. Hu, D. Kholodenko, R. C. Malenka, R. A. Nicoll and L. Mucke, *Proc. Natl. Acad. Sci. USA*, 1999, **96**, 3228-3233.
7. Y. Miller, B. Ma and R. Nussinov, *Chem. Rev.*, 2010, **110**, 4820-4838.
8. K. Ono, M. M. Condron and D. B. Teplow, *Proc. Natl. Acad. Sci. U. S. A.*, 2009, **106**, 14745-14750.
9. S. Lesné, M. T. Koh, L. Kotilinek, R. Kayed, C. G. Glabe, A. Yang, M. Gallagher and K. H. Ashe, *Nature*, 2006, **440**, 352-357.
10. M. Townsend, G. M. Shankar, T. Mehta, D. M. Walsh and D. J. Selkoe, *J. Physiol.*, 2006, **572**, 477-492.
11. G. M. Shankar, S. Li, T. H. Mehta, A. Garcia-Munoz, N. E. Shepardson, I. Smith, F. M. Brett, M. A. Farrell, M. J. Rowan, C. A. Lemere, C. M. Regan, D. M. Walsh, B. L. Sabatini and D. J. Selkoe, *Nat. Med.*, 2008, **14**, 837-842.
12. A. Quist, I. Doudevski, H. Lin, R. Azimova, D. Ng, B. Frangione, B. Kagan, J. Ghiso and R. Lal, *Proc. Natl. Acad. Sci. U. S. A.*, 2005, **102**, 10427-10432.
13. Z. Jaunmuktane, S. Mead, M. Ellis, J. D. Wadsworth, A. J. Nicoll, J. Kenny, F. Launchbury, J. Linehan, A. Richard-Loendt, A. S. Walker, P. Rudge, J. Collinge and S. Brandner, *Nature*, 2015, **525**, 247-250.
14. D. E. Ehrnhoefer, J. Bieschke, A. Boeddrich, M. Herbst, L. Masino, R. Lurz, S. Engemann, A. Pastore and E. E. Wanker, *Nat. Struct. Mol. Biol.*, 2008, **15**, 558-566.
15. A. R. A. Ladiwala, J. S. Dordick and P. M. Tessier, *J. Biol. Chem.*, 2011, **286**, 3209-3218.
16. S. L. Bernstein, N. F. Dupuis, N. D. Lazo, T. Wyttenbach, M. M. Condron, G. Bitan, D. B. Teplow, J.-E. Shea, B. T. Ruotolo, C. V. Robinson and M. T. Bowers, *Nat. Chem.*, 2009, **1**, 326-331.
17. N. J. Economou, M. J. Giammona, T. D. Do, X. Zheng, D. B. Teplow, S. K. Buratto and M. T. Bowers, *J. Am. Chem. Soc.*, 2016, **138**, 1772-1775.
18. S. I. A. Cohen, S. Linse, L. M. Luheshi, E. Hellstrand, D. A. White, L. Rajah, D. E. Otzen, M. Vendruscolo, C. M. Dobson and T. P. J. Knowles, *Proc. Natl. Acad. Sci. U.S.A.*, 2013, **110**, 9758-9763.
19. C. Liang, R. Ni, J. E. Smith, W. S. Childers, A. K. Mehta, and D. G. Lynn, *J. Am. Chem. Soc*., 2014, **136**, 15146-15149.

20. S. Chimon, M. A. Shaibat, C. R. Jones, D. C. Calero, B. Aizezi and Y. Ishii, *Nat. Struct. Mol. Biol.*, 2007, **14**, 1157-1164.

21. M. Ahmed, J. Davis, D. Aucoin, T. Sato, S. Ahuja, S. Aimoto, J. I. Elliott, W. E. Van Nostrand and S. O. Smith, *Nat. Struct. Mol. Biol.*, 2010, **17**, 561-567.

22. J. D. Pham, N. Chim, C. W. Goulding and J. S. Nowick, *J. Am. Chem. Soc.*, 2013, **135**, 12460-12467.

23. H. Ding, P. T. Wong, E. L. Lee, A. Gafni and D. G. Steel, *Biophys. J.*, 2009, **97**, 912-921.

24. T. M. Ryan, N. Kirby, H.D. T. Mertens, B. Roberts, K. J. Barnham, R. Cappai, C. L. L. Pham, C. L. Masters and C. C. Curtain, *Metallomics*, 2015, **7**, 536-543.

25. Y. Miller, B. Ma, C.-J. Tsai and R. Nussinov, *Proc. Natl. Acad. Sci. U. S. A.*, 2010, **107**, 14128-14133.

26. S.-J. Hyung, A. S. DeToma, J. R. Brender, S. Lee, S. Vivekanandan, A. Kochi, J.-S. Choi, A. Ramamoorthy, B. T. Ruotolo and M. H. Lim, *Proc. Natl. Acad. Sci. U. S. A.*, 2013, **110**, 3743-3748.

27. J. S. Derrick, R. A. Kerr, Y. Nam, S. B. Oh, H. J. Lee, K. G. Earnest, N. Suh, K. L. Peck, M. Ozbil, K. J. Korshavn, A. Ramamoorthy, R. Prabhakar, E. J. Merino, J. Shearer, J.-Y. Lee, B. T. Ruotolo and M. H. Lim, *J. Am. Chem. Soc.*, 2015, **137**, 14785-14797.

28. M. F. M. Sciacca, S. A. Kotler, J. R. Brender, J. Chen, D.-k. Lee and A. Ramamoorthy, *Biophys. J.*, 2012, **103**, 702-710.

29. C. L. Teoh, D. Su, S. Sahu, S.-W. Yun, E. Drummond, F. Prelli, S. Lim, S. Cho, S. Ham, T. Wisniewski and Y.-T. Chang, *J. Am. Chem. Soc.*, 2015, **137**, 13503-13509.

30. R. Kayed, E. Head, J. L. Thompson, T. M. McIntire, S. C. Milton, C. W. Cotman and C. G. Glabe, *Science*, 2003, **300**, 486-489.

31. I. Morgado, K. Wieligmann, M. Bereza, R. Rönicke, K. Meinhardt, K. Annamalai, M. Baumann, J. Wacker, P. Hortschansky, M. Malešević, C. Parthier, C. Mawrin, C. Schiene-Fischer, K. G. Reymann, M. T. Stubbs, J. Balbach, M. Görlach, U. Horn and M. Fändrich, *Proc. Natl. Acad. Sci. U. S. A.*, 2012, **109**, 12503-12508.

32. T. Kawarabayashi, M. Shoji, L. H. Younkin, L. Wen-Lang, D. W. Dickson, T. Murakami, E. Matsubara, K. Abe, K. H. Ashe and S. G. Younkin, *J. Neurosci.*, 2004, **24**, 3801-3809.

33. S. Hong, Beth L. Ostaszewski, T. Yang, Tiernan T. O′Malley, M. Jin, K. Yanagisawa, S. Li, T. Bartels and D. J. Selkoe, *Neuron*, 2014, **82**, 308-319.

34. M. Talantova, S. Sanz-Blasco, X. Zhang, P. Xia, M. W. Akhtar, S.-i. Okamoto, G. Dziewczapolski, T. Nakamura, G. Cao, A. E. Pratt, Y.-J. Kang, S. Tu, E. Molokanova, S. R. McKercher, S. A. Hires, H. Sason, D. G. Stouffer, M. W. Buczynski, J. P. Solomon, S. Michael, E. T. Powers, J. W. Kelly, A. Roberts, G. Tong, T. Fang-Newmeyer, J. Parker, E. A.

Holland, D. Zhang, N. Nakanishi, H.-S. V. Chen, H. Wolosker, Y. Wang, L. H. Parsons, R. Ambasudhan, E. Masliah, S. F. Heinemann, J. C. Piña-Crespo and S. A. Lipton, *Proc. Natl. Acad. Sci. U. S. A.*, 2013, **110**, E2518-E2527.

35. J. W. Um, H. B. Nygaard, J. K. Heiss, M. A. Kostylev, M. Stagi, A. Vortmeyer, T. Wisniewski, E. C. Gunther and S. M. Strittmatter, *Nat Neurosci*, 2012, **15**, 1227-1235.
36. A. Y. Lai and J. McLaurin, *Int. J. Alzheimers Dis.*, 2011, **2011**, Article ID: 548380.
37. E. Cerf, R. Sarroukh, S. Tamamizu-Kato, L. Breydo, S. Derclaye, Yves F. Dufrêne, V. Narayanaswami, E. Goormaghtigh, J.-M. Ruysschaert and V. Raussens, *Biochem. J.*, 2009, **421**, 415-423.
38. T. Umeda, T. Tomiyama, N. Sakama, S. Tanaka, M. P. Lambert, W. L. Klein and H. Mori, *J. Neurosci. Res*, 2011, **89**, 1031-1042.
39. R. Resende, E. Ferreiro, C. Pereira, and C. Resende de Oliveira, *Neuroscience*, 2008, **155**, 725-737.
40. D.-H. Cho, T. Nakamura, J. Fang, P. Cieplak, A. Godzik, Z. Gu and S. A. Lipton, *Science*, 2009, **324**, 102-105.
41. W. W. Poon, A. J. Carlos, B. L. Aguilar, N. C. Berchtold, C. K. Kawano, V. Zograbyan, T. Yaopruke, M. Shelanski and C. W. Cotman, *J. Biol. Chem.*, 2013, **288**, 16937-16948.
42. J. Domert, S. B. Rao, L. Agholme, A.-C. Brorsson, J. Marcusson, M. Hallbeck and S. Nath, *Neurobiol. Dis.*, 2014, **65**, 82-92.
43. K. Ono, L. Li, Y. Takamura, Y. Yoshiike, L. Zhu, F. Han, X. Mao, T. Ikeda, J.-i. Takasaki, H. Nishijo, A. Takashima, D. B. Teplow, M. G. Zagorski and M. Yamada, *J. Biol. Chem.*, 2012, **287**, 14631-14643.
44. A. Frydman-Marom, M. Rechter, I. Shefler, Y. Bram, D. E. Shalev and E. Gazit, *Angew. Chem. Int. Ed.*, 2009, **48**, 1981-1986.
45. S. Sinha, D. H. J. Lopes, Z. Du, E. S. Pang, A. Shanmugam, A. Lomakin, P. Talbiersky, A. Tennstaedt, K. McDaniel, R. Bakshi, P.-Y. Kuo, M. Ehrmann, G. B. Benedek, J. A. Loo, F.-G. Klärner, T. Schrader, C. Wang and G. Bitan, *J. Am. Chem. Soc.*, 2011, **133**, 16958-16969.
46. M. W. Beck, S. B. Oh, R. A. Kerr, H. J. Lee, S. H. Kim, S. Kim, M. Jang, B. T. Ruotolo, J.-Y. Lee and M. H. Lim, *Chem. Sci*., 2015, **6**, 1879-1886.
47. S. I. A. Cohen, P. Arosio, J. Presto, F. R. Kurudenkandy, H. Biverstål, L. Dolfe, C. Dunning, X. Yang, B. Frohm, M. Vendruscolo, J. Johansson, C. M. Dobson, A. Fisahn, T. P. J. Knowles and S. Linse, *Nat. Struct. Mol. Biol.*, 2015, **22**, 207-213.
48. J. A. Lenhart, X. Ling, R. Gandhi, T. L. Guo, P. M. Gerk, D. H. Brunzell and S. Zhang, *J. Med. Chem.*, 2010, **53**, 6198-6209.
49. J.-S. Choi, J. J. Braymer, R. P. R. Nanga, A. Ramamoorthy and M. H. Lim, *Proc. Natl. Acad. Sci. U. S. A.*, 2010, **107**, 21990-21995.

50. A. R. A. Ladiwala, M. Bhattacharya, J. M. Perchiacca, P. Cao, D. P. Raleigh, A. Abedini, A. M. Schmidt, J. Varkey, R. Langen and P. M. Tessier, *Proc. Natl. Acad. Sci. U. S. A.*, 2012, **109**, 19965-19970.

51. M. Sato, K. Murakami, M. Ono, Y. Nakagawa, S. Katayama, K-I. Akagi, Y. Masuda, K. Takegoshi, and K. Irie, *J. Biol. Chem*., 2013, **288**, 23212-23224.

Chapter 2.

Oxidative Transformations of Dopamine Determine its Regulatory Activities against Pathological Features in Alzheimer's Disease

I thank Jeffrey S. Derrick for performing the studies using TEM, cyclic voltammetry, and spectroelectrochemistry and Shin Jung C. Lee for conducting the mass spectrometric experiments. I carried out the experiments using gel/Western blot and UV-vis spectroscopy, and analyzed data from ESI-MS, IM-MS, and MS/MS.

2.1. Introduction

Dopamine (**DA**), a neurotransmitter to long-term memory and motor activity in the brain,[1] is shown to be rapidly oxidized with generation of reactive oxygen species (ROS) even under physiological conditions.[2-6] Spontaneous oxidation of **DA** produces its various transfigured forms as shown in Scheme 2.1. Formation of dopamine-*o*-quinone (**DQ**) causes rapid cyclization affording leucoaminochrome (**LC**), aminochrome (**AC**), 5,6-dihydroxyindole (**HI**), and 5,6-indolequinone (**IQ**).[2,3] During oxidation processes of **DA**, **HI** or **IQ** can be polymerized to neuromelanin[2,3] and ROS, such as superoxide anions($O_2^{\bullet-}$), can be generated.[2,4] Since ROS overgeneration is associated with oxidative stress, it has been presented that **DA**'s oxidation could trigger harmful effects potentially leading to the pathogenesis of brain diseases.[2,3] On the contrary, some perspective has indicated protective effects of **DA**'s oxidation.[5,6] For example, one of the products (*i.e.*, neuromelanin) upon **DA**'s oxidation is an antioxidant sequestering redox-active metals.[5,6] The link of **DA**'s oxidation particularly to pathological pathways in the brain remains elusive, however.

Scheme 2.1. Proposed oxidative transformations of **DA**.

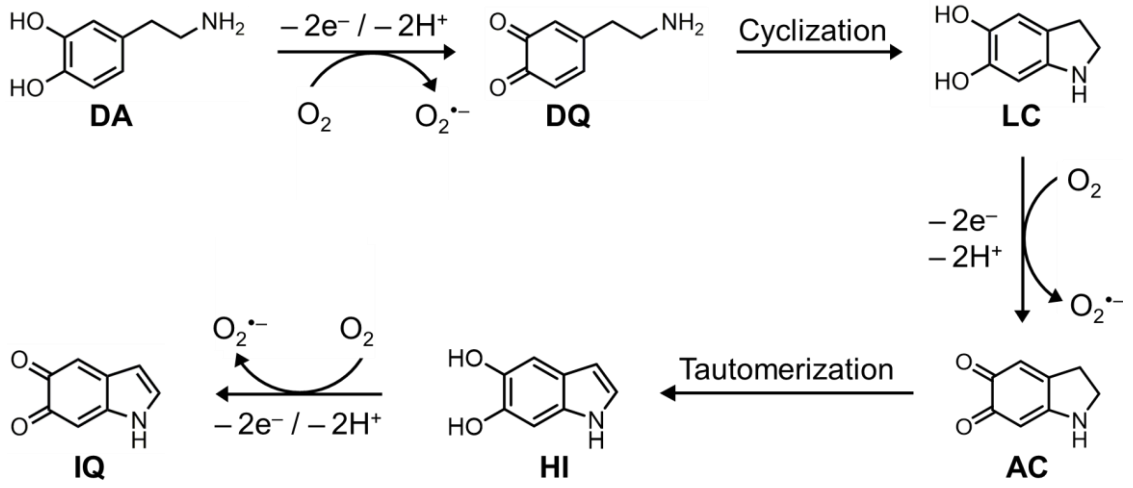

Various studies have demonstrated the connection of **DA** with amyloid-related diseases [*e.g.*, Alzheimer's disease (AD), Parkinson's disease].[2,3,7] One of the amyloid-related diseases, AD, is characterized by amyloid-β (Aβ) peptide aggregation, metal ion dyshomeostasis, and oxidative stress.[8] **DA** has been suggested to be correlated with these pathological components *via* its oxidative processes; (i) along with co-localization of Aβ in dopaminergic systems resulting in neurodegeneration:[9] (ii) prevention of metal-free Aβ aggregation through **DA**'s oxidation;[7] (iii) redox-active metal-mediated oxidation of **DA**;[2,10] (iv) production of ROS.[2,4,11,12] Multiple questions regarding the effects of such interactions and reactions of **DA** with multiple pathological factors found

in AD towards the disease pathogenesis are still unclear, however. For instance, the key oxidation process of **DA**, responsible for controlling metal-free Aβ aggregation, has not been fully understood.[2,3,7] Until now, the interaction of **AC** (Scheme 2.1) with Aβ has been suggested as an active form of preventing Aβ aggregation.[7] The covalent adduct formations between **DQ** (Scheme 2.1) and amyloid proteins as well as peptide oxidation by **DA** have been indicated from the studies between **DA** and another amyloid protein (*i.e.*, α-synuclein), but not Aβ.[2,3,7,13] In addition, the influence of **DA** on modulation of metal-induced Aβ aggregation has not been reported. Moreover, controversial results have been presented about **DA** towards oxidative stress in the brain, since ROS could function as signaling factors in biological systems as well as inducers for oxidative stress, depending on their concentrations.[2,5,6,10-12]

Herein, we report the regulatory effects of **DA** towards AD pathological components, such as metal-free Aβ, metal-bound Aβ, and ROS through its oxidative transformations. The oxidative processes of **DA** are shown to significantly affect both metal-free Aβ and metal-bound Aβ aggregation pathways inducing nontoxic, amorphous off-pathway peptide species. Mass spectrometric (MS) studies indicate the oxidation of the amino acid residues of Aβ, such as methionine 35 (Met35), upon **DA**'s oxidation. Such peptide oxidation triggered by ROS generation *via* **DA**'s oxidative transformations could be a mechanism to modulate Aβ aggregation. In addition, employing a chemical library composed of six different structural analogues with different degrees of oxidation, produced from variations of **DA**'s framework, **DA**'s oxidation is confirmed to be critical for its activities with the pathological factors. Taken together, our overall studies demonstrate the neuroprotection by **DA** towards pathological factors found in AD.

2.2. Results and Discussion

2.2.1. Effects of DA on Modulation of Metal-free Aβ and Metal-induced Aβ Aggregation *In Vitro*

In order to investigate the ability of **DA** to modulate Aβ in the absence and presence of metal ions [*i.e.*, Cu(II), Zn(II)], gel electrophoresis with Western blotting (gel/Western blot) and transmission electron microscopy (TEM) were carried out to observe the molecular weight (MW) distribution and morphological changes of the resultant Aβ species, respectively. Two different of experiments were performed using gel/Western blot, as shown in Figures 2.1 and 2.2: (i) Ability of **DA** to prevent Aβ aggregation was tested by inhibition experiments (Figure 2.1) and (ii) its capability of disassembling preformed aggregates was examined by disaggregation experiments (Figure 2.2). During the incubation, Aβ peptides aggregate and generate large, insoluble aggregates[8] that are detected by TEM, but too large to penetrate the gel matrix; therefore, only small sizes of Aβ species are observed in the gel/Western blot. When Aβ aggregation is inhibited or redirected, various sizes of Aβ species permeable through gel matrix can be indicated by smearing a band throughout the lane of gel/Western

blot using an anti-Aβ antibody (6E10). In the inhibition experiment, different MW distributions were observed for both metal-free $A\beta_{40}$ and metal-bound $A\beta_{40}$ species upon treatment with **DA**. (Figure 2.1b; top), TEM images of the resultant metal-free $A\beta_{42}$ and metal-bound $A\beta_{42}$ aggregates generated by addition with **DA** showed the morphological changes from large fibril-like aggregates to small, amorphous aggregates, demonstrating the consistent results with gel/Western blot (Figure 2.1c). On the other hand, under anaerobic conditions, the treatment of **DA** with Aβ results in no discernible changes in gel/Western blot compared to **DA**-untreated metal-free $A\beta_{40}$ and metal–$A\beta_{40}$ (Figure 2.1b; bottom).

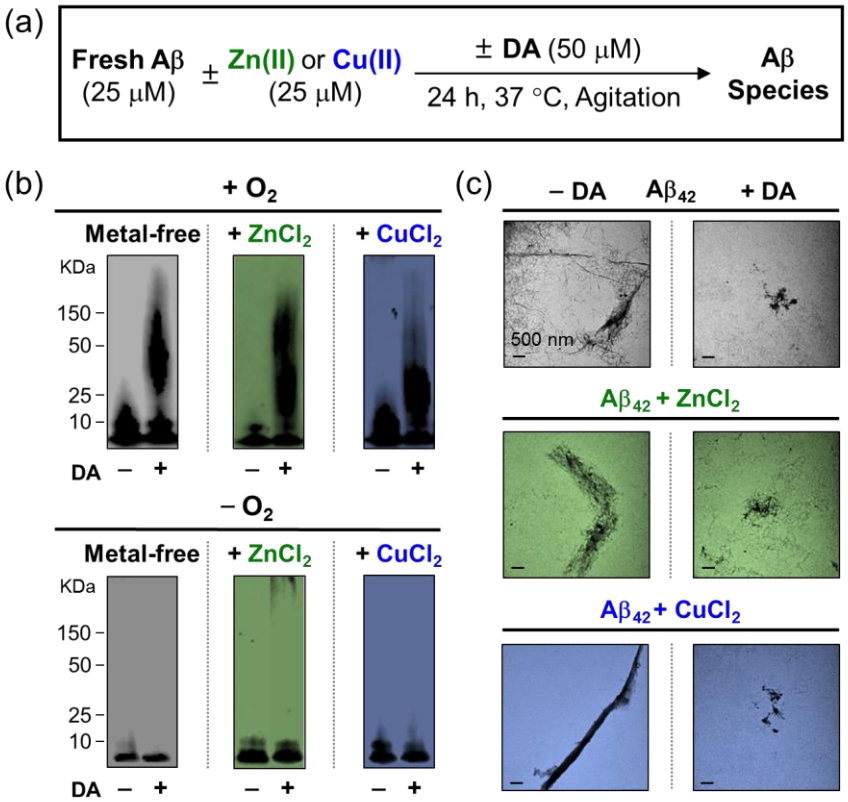

Figure 2.1. Inhibitory effects of **DA** on both metal-free and metal-induced Aβ aggregation in the presence and absence of O_2. (a) Scheme of inhibition experiments. (b) Visualization of the size-distribution of the resultant Aβ species with and without **DA** treatment under aerobic (top) and anaerobic (bottom) conditions. (c) TEM images of the resultant metal-free $A\beta_{42}$ and metal–$A\beta_{42}$ aggregates from the 24 h incubated samples. The scale bar is 500 nm. Experimental conditions: [$A\beta_{40}$ or $A\beta_{42}$] = 25 μM; [$ZnCl_2$ or $CuCl_2$] = 25 μM; [**DA**] = 50 μM; pH 6.6 (for Cu(II) samples) or pH 7.4 (for metal-free and Zn(II) samples); 37 °C; 24 h incubation; constant agitation.

The capacity of **DA** to dismantle preformed metal-free Aβ and metal-treated Aβ aggregates was also revealed by disaggregation experiments (Figure 2.2). After Aβ was preincubated with or without metal ions [*i.e.*, Zn(II) or Cu(II)] for aggregation, **DA** was treated to preformed Aβ aggregates.

Similar to the results obtained from inhibition experiments under aerobic conditions, **DA** had the noticeable reactivity toward preformed metal-free and metal-induced Aβ aggregates. Discernible smearing bands were observed at all conditions except sample containing the metal-free $A\beta_{42}$ aggregates. Overall, our *in vitro* gel/Western blot and TEM studies suggest that (i) **DA** could inhibit and disassemble both metal-free Aβ and metal-induced Aβ aggregation generating amorphous species; (ii) O_2 is indicated to play an important role in **DA**'s controlling reactivity with Aβ peptides.

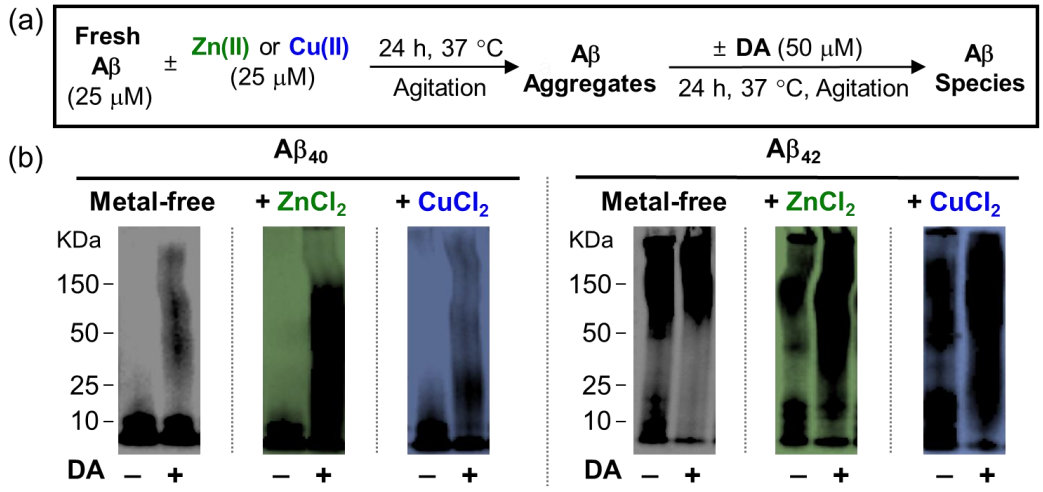

Figure 2.2. Capability of **DA** to disaggregate preformed metal-free and metal-treated Aβ aggregates. (a) Scheme of disaggregation experiments. (b) Visualization of the size-distribution of $A\beta_{40}$ (left) and $A\beta_{42}$ (right) species with and without **DA** treatment. Experimental conditions: [$A\beta_{40}$ or $A\beta_{42}$] = 25 μM; [$ZnCl_2$ or $CuCl_2$] = 25 μM; [**DA**] = 50 μM; pH 6.6 (for Cu(II) samples) or pH 7.4 (for metal-free and Zn(II) samples); 37 °C; 24 h incubation; constant agitation.

2.2.2. Oxidation of Aβ by DA

The reactivity of **DA** toward both metal-free Aβ and metal-induced Aβ aggregation pathways was further probed by electrospray ionization mass spectrometry (ESI-MS) combined with ion mobility-mass spectrometry (IM-MS) (Figure 2.3). When **DA** was incubated with metal-free $A\beta_{40}$, in addition to the $A\beta_{40}^{4+}$ monomer peak at 1083.2 *m/z*, a new peak at 1087.3 *m/z* (corresponding to the addition of an oxygen atom to $A\beta_{40}^{4+}$ monomer) was observed (Figure 2.3a; the peak marked in a red dot). IM-MS studies of the 4^+ charge state presented that the oxidized $A\beta_{40}$ monomer had the distinct ion mobility (IM) time (Figure 2.3b; collisional cross section data in Table 2.1) compared to the $A\beta_{40}$ monomer. The oxidized $A\beta_{40}$ monomer indicated decreased ion mobility (IM) arrival time, suggesting its more conformational compaction and role in altering Aβ aggregation pathways, consequently. In the presence of Cu(II), oxidation of $A\beta_{40}$ also occurred after treatment of **DA**, showing peaks corresponding to the addition of one, two and three oxygen atoms to $A\beta_{40}$ (Figure 2.3c).

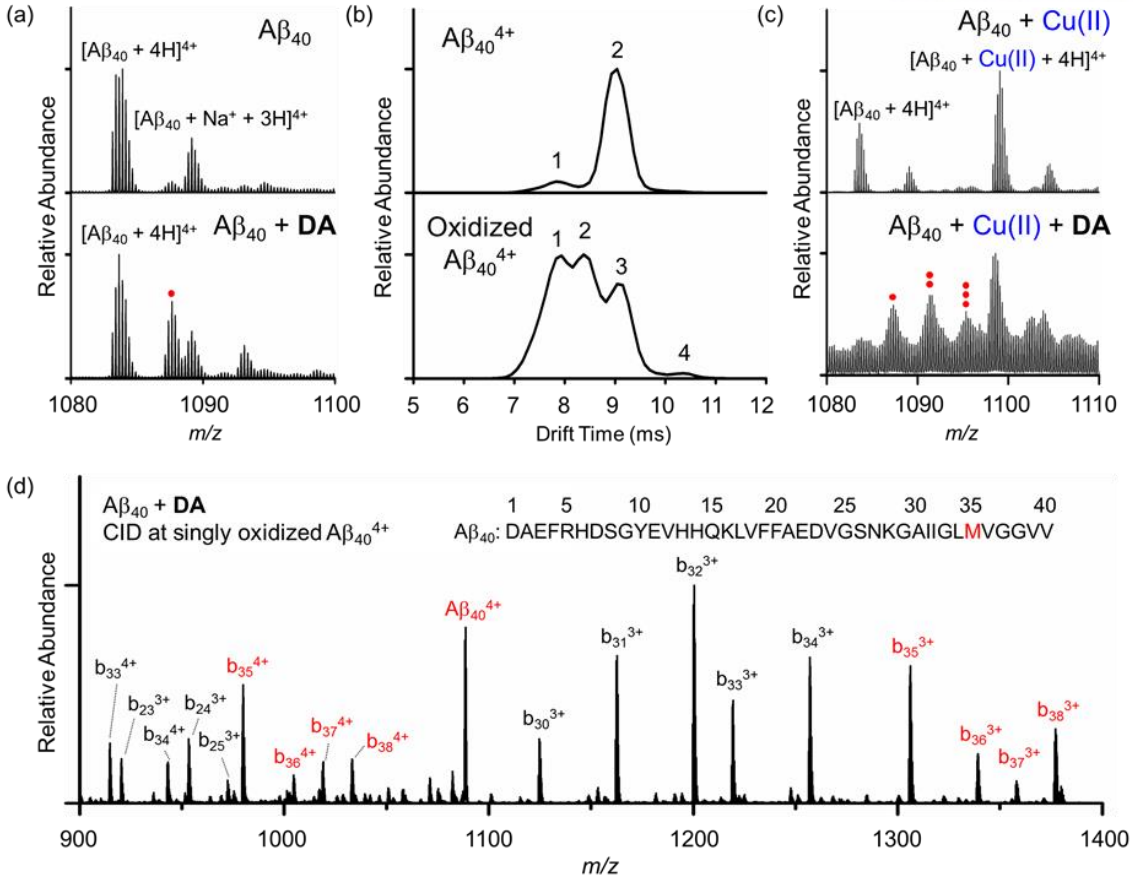

Figure 2.3. Mass spectrometric analyses of $A\beta_{40}$ monomers upon treatment with **DA**. The addition of an oxygen atom is marked in a red dot. (a) Mass spectrometric analysis showing $A\beta_{40}$ oxidation in the presence of **DA**. (b) Arrival time distribution (ATD) of the singly oxidized $A\beta_{40}^{4+}$ peak $[A\beta_{40} + O + 4H]^{4+}$. Collision cross section (CCS) values for all ion mobility data sets are presented in Table 2.1. (c) Mass spectrometric analysis of $A\beta_{40}$ monomers with **DA** and $CuCl_2$. (d) MS/MS sequencing of the oxidized $A\beta_{40}^{4+}$ peak $[A\beta_{40} + O + 4H]^{4+}$. Experimental conditions: $[A\beta_{40}]$ = 100 μM; $[CuCl_2]$ = 100 μM; [compound] = 500 μM; pH 7.5; 37 °C; 6 h incubation (for metal-free samples) or 1 h incubation (for Cu(II) samples); 100 mM ammonium acetate. Incubated samples were diluted by 10-fold before injection into the mass spectrometer.

Table 2.1. Calculated collision cross section (CCS) data from singly oxidized $A\beta_{40}^{4+}$ monomer species

		Conformational Species (Å^2)			
		1	2	3	4
$A\beta_{40}$	$[A\beta_{40} + 4H]^{4+}$	662.75	727.45	-	-
$A\beta_{40}$ + **DA**	$[A\beta_{40} + O + 4H]^{4+}$	668.77	692.60	727.44	794.22

To investigate the amino acid residues of Aβ that are oxidized by **DA** treatment, tandem MS/MS in conjunction with collision-induced dissociation (CID) for the singly oxidized $A\beta_{40}$ was performed

to investigate amino acid residues responsible for the Aβ oxidation. Our studies indicated that **DA** could trigger the oxidation of the Met35 residue of $A\beta_{40}$ (Figure 2.3d). The Met oxidation has been linked to the delay of Aβ aggregation pathways[14,15] and could generate oligomeric forms different from toxic, structured oligomers.[16,17] Since the toxicity of Aβ oligomers could be caused by their structures,[18,19] unstructured, amorphous oligomers are relatively nontoxic.[20,21] In addition, retardation of amyloidogenic aggregation could prevent the production of oligomers induced by fibril fragmentation.[22] Thus, the overall aspects have made us consider the nontoxic effects of the Met35-oxidized Aβ by **DA**. Upon treatment of Aβ with both Cu(II) and **DA,** more oxidation to amino acid residues of Aβ (not only Met35) was observed. Note that the relative abundance of oxidized Aβ species were too low to be further analyzed (the data is not shown). Overall, our ESI-MS, IM-MS, and tandem MS/MS studies demonstrate that **DA**'s regulatory reactivity with aggregation of metal-free and metal-bound Aβ is suggested to be resulted from its mediation for Aβ oxidation.

2.2.3. Oxidative Transformations of DA Facilitated by Aβ, Cu(II), and Cu(II)-treated Aβ

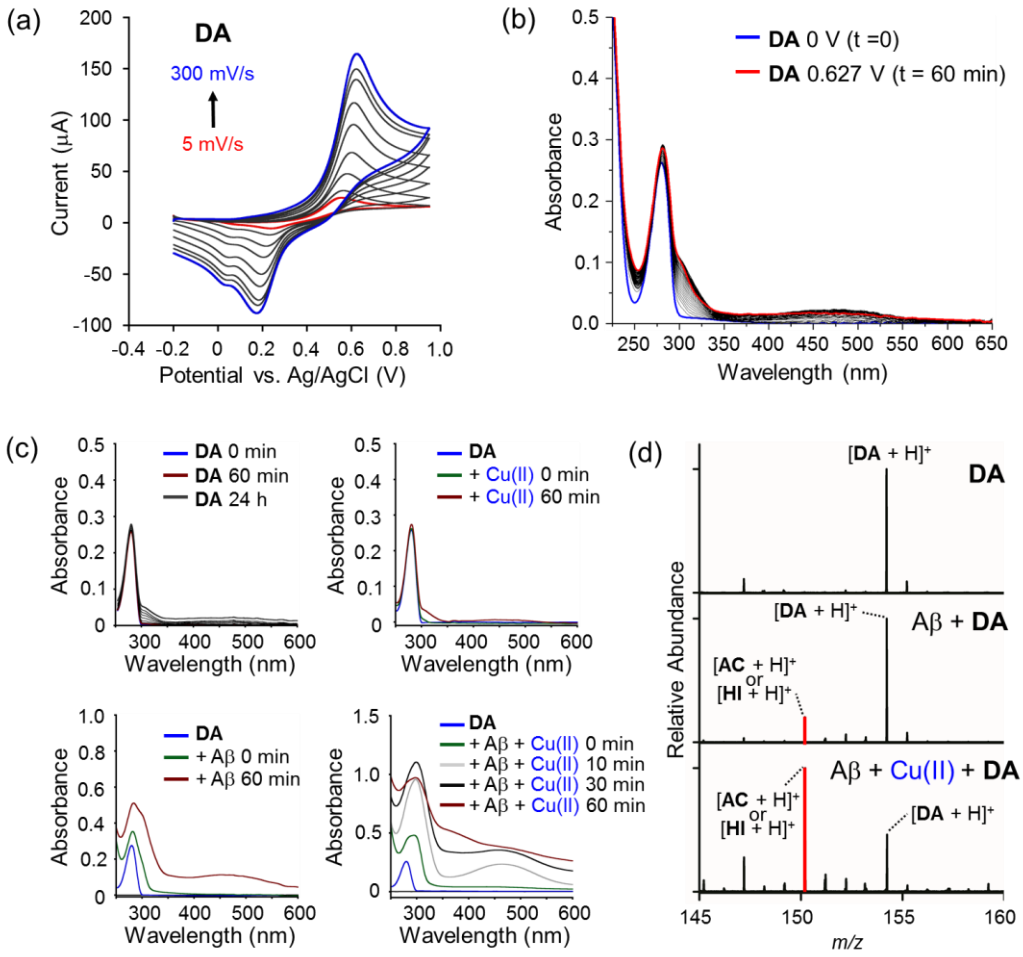

Figure 2.4. Oxidative transformations of **DA**. (a) Electrochemical analysis of **DA**. Cyclic

voltammograms of **DA** in H_2O with 1 M NaCl as a supporting electrolyte at variable scan rates (5, 10, 25, 50, 100, 150, 200, 250, and 300 mV/s). (b) Spectroelectrochemical investigations of **DA** (0.627 V). Potentials were reported and collected *versus* the Ag/AgCl couple. (c) Transformations of **DA** with or without $CuCl_2$ and/or $A\beta_{40}$, monitored by UV-vis spectroscopy. Experimental conditions: [$A\beta_{40}$] = 50 μM; [$CuCl_2$] = 50 μM; [compound] = 100 μM, pH 6.6 (for Cu(II) samples) or pH 7.4 (for metal-free samples); 37 °C; 1 h incubation; no agitation. (d) **DA's** transfigurations with or without $CuCl_2$ and/or $A\beta_{40}$ measured by mass spectrometry. Experimental conditions: [$A\beta_{40}$] = 100 μM; [$CuCl_2$] = 100 μM; [compound] = 500 μM; 100 mM ammonium acetate; pH 7.5; 37 °C; 1 h incubation; no agitation. Incubated samples were diluted by 10-fold before injection into the mass spectrometer.

To further probe how **DA** controls the aggregation pathways of metal-free and metal-bound Aβ, interactions of **DA** with Aβ in the absence and presence of metals were analyzed under various conditions (Figure 2.4). The redox potential of **DA** was first investigated by cyclic voltammetry in H_2O (Figure 2.4a and Table 2.2). The irreversible oxidation wave with the peak anodic potential (E_{pa}) at *ca.* 0.627 V was revealed from **DA**. To identify optical features upon oxidation of **DA**, spectroelectrochemistry was carried out applying the peak anodic potential obtained from cyclic voltammetry. The optical bands at *ca*. 308 nm and 475 nm, previously assigned to oxidative transfiguration of **DA** to **AC**,[3,23-25] appeared over 60 min incubation followed by generation of black precipitates possibly associated with formation of neuromelanin by polymerization of **HI** or **IQ** (Scheme 2.1) (UV data not shown).[3,23] Optical bands corresponding to **DQ** (*i.e*., *ca*. 308 nm and 350 nm), an intermediate product between **DA** and **AC** (Scheme 2.1), were not detected, which may be a result of its unstable property and rapid cyclization to **AC**.[2,3,23]

The optical spectra of **DA** with or without $A\beta_{40}$ in the presence or absence of Cu(II) were monitored by UV-vis spectroscopy (Figure 2.4c). Upon incubation of **DA** in a buffer solution, the optical bands gradually appeared at *ca.* 308 nm and 475 nm for 24 h, indicative of the formation of **AC**.[3, 22-24] The optical spectrum of **DA** was stable at *ca.* 280 nm for 1 h incubation. When **DA** was incubated with Cu(II) or $A\beta_{40}$, the spectra corresponding to **AC** were observed within 1 h. Upon addition of both $A\beta_{40}$ and Cu(II), the oxidative transformations of **DA** were shown to be accelerated. The peak matched with the cyclized form of **DA** was directly indicated within 10 min. After identification of the **DA**'s oxidative transformations in the presence of metal-free $A\beta_{40}$, Cu(II), and Cu(II)-treated $A\beta_{40}$ by UV-vis spectroscopy, ESI-MS was applied to examine its transformed products. This study supported the findings obtained from our UV-vis experiments by detecting peaks corresponding to the oxidized products of **DA** (Figure 2.4d). In a similar manner, **DA** was incubated with or without $A\beta_{40}$ in the absence or presence of Cu(II) for 1 h. Only a peak at 154 *m/z* coincided with the [**DA** + H]$^+$ appeared from **DA** incubated without both $A\beta_{40}$ and Cu(II). When **DA** was incubated with $A\beta_{40}$, in addition to the peak assigned to the [**DA** + H]$^+$, a peak at 150 *m/z* associated with the [**AC** + H]$^+$ or [**HI** + H]$^+$ was represented, which could suggest the **DA**'s cyclization by its

oxidation. Upon addition of Cu(II), a generation of the peak at 150 *m/z* was observed with higher relative abundance than the peak from the incubation of **DA** only with $A\beta_{40}$. These results could explain that the cyclization of **DA** *via* its oxidative transformations is linked to its modulating activity toward metal-free and Cu(II)-induced Aβ aggregation.

2.2.4. Rational Selection of DA Derivatives

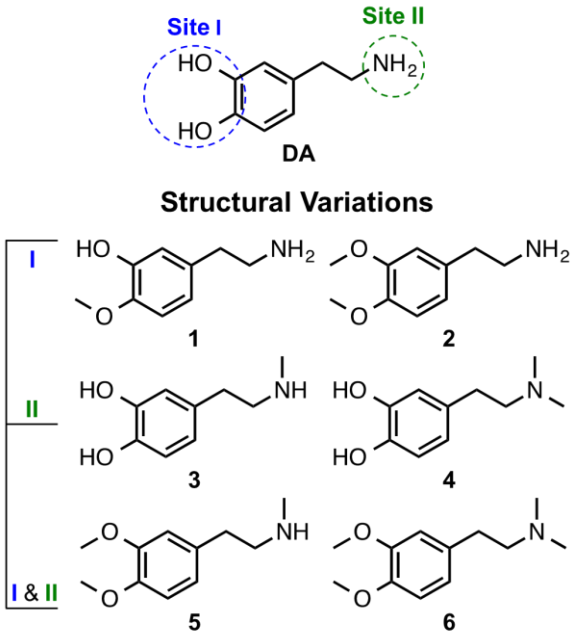

Figure 2.5. Derivatives of **DA**. The catechol moiety (Site I) was systematically altered to monomethoxy or dimethoxy functionality. The primary amino group of **DA** (Site II) was varied with a monomethylamino or dimethylamino group.

In order to elucidate **DA**'s regulatory effects on metal-free and Cu(II)-induced Aβ aggregation *via* its oxidative transformations, structure-reactivity studies were carried out employing our six different **DA** derivatives. These **DA** derivatives were designed based on the structural modifications of **DA** (Figure 2.5). To identify the importance of **DA**'s initial oxidation on its reactivity toward metal-free and metal-bound Aβ aggregation, a catechol moiety (Site I), critical for the initial oxidation of **DA** to **DQ**,[2,3] was modified to a monomethoxy (**1**) or dimethoxy group (**2**). The oxidative transformations from **DQ** to cyclized products (*e.g.*, **LC**, **AC**, **HI, IQ**; Scheme 2.1**)** occur by a nucleophilic attack of the deprotonated side amino group (Site II of **DA**) to the electron-deficient quinone ring,[2,3] thus, the role of oxidative cyclization of **DA** toward modulation of metal-free and Cu(II)-induced Aβ aggregation was investigated by substitution of the amino group (Site II) to a methylamino (**3**) or a dimethylamino group (**4**). Both Site I and Site II were changed to dimethoxy and methylamino groups (**5**) or dimethylamino functionality (**6**) for comparison of the reactivity with **3** and **4**.

2.2.5. Reactivity of DA Derivatives with Metal-free and Metal-bound Aβ species

Redox potentials of DA derivatives. The redox potentials of six derivatives (Figure 2.5) were measured and compared with that of **DA** to analyze **DA**'s electrochemical behavior by cyclic voltammetry (CV). Except for **6**, which indicated two quasi-reversible redox couples, only compounds equipped with the catechol moiety (*i.e.*, **3** and **4**) revealed similar results with **DA** showing irreversible oxidation waves with E_{pa} at *ca*. 0.657 V and 0.647 V, respectively (Figure 2.6). Compounds **1**, **2**, and **5** were relatively inert toward oxidation compared to **DA**. No significant anodic currents were generated until much more positive potentials were applied (*ca.* 0.80 V). The peak anodic potentials of **1**, **2**, and **5** were higher than **3**, **4**, and **DA**, thus suggesting that the oxidation could easily occur from the catechol-included compounds (Figure 2.6). Although **6** with 3,4-dimethyoxy functionality showed two quasi-reversible redox couples, the peak anodic current (i_{pa}) was much lower than that of **DA**, **3**, and **4**, suggesting that a relatively small amount of **6** could undergo its oxidative transformations compared to the catechol containing **DA** derivatives. Collectively, our electrochemical studies suggest that the catechol functionality is essential for significant oxidative transformations of **DA**.

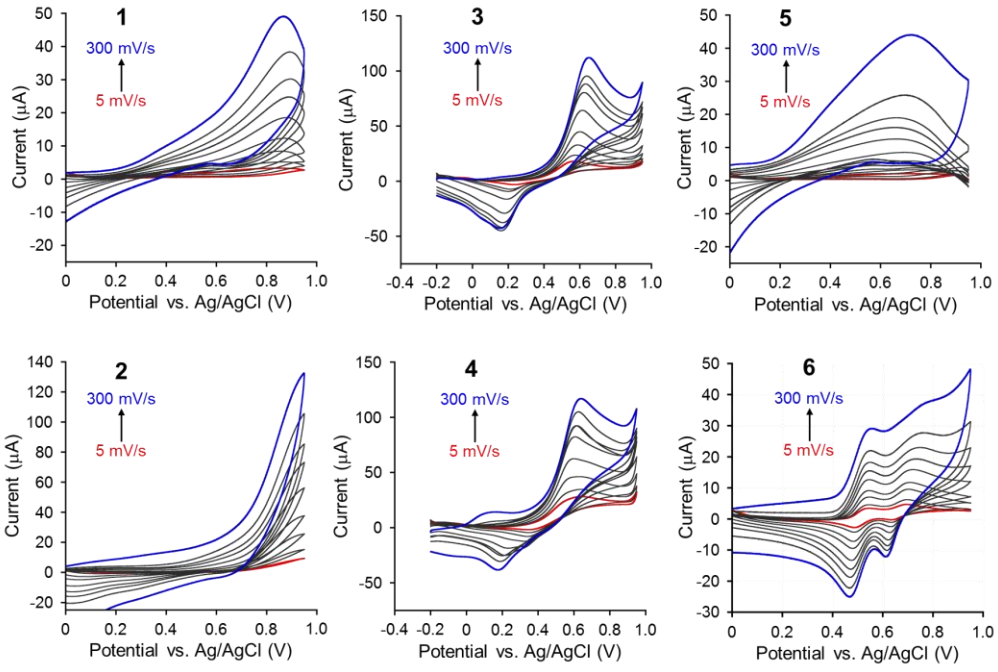

Figure 2.6. Cyclic voltammograms of **DA**'s derivatives in H_2O with 1 M NaCl as a supporting electrolyte at variable scan rates (5, 10, 25, 50, 100, 150, 200, 250, and 300 mV/s).

Table 2.2. Electrochemical parameters obtained from the cyclic voltammograms of **DA** and its derivatives.

ν (mV/s)	E_{pa1} (V)	E_{pa2} (v)	E_{pc1} (v)	E_{pc2} (V)	i_{pa1} (μA)	i_{pa2} (μA)	i_{pc1} (μA)	i_{pc2} (μA)
				DA				
5	–	0.555	–	0.238	–	22.01	–	-2.26
10	–	0.563	–	0.231	–	27.90	–	-5.63
25	–	0.580	–	0.217	–	42.28	–	-12.92
50	–	0.601	–	0.206	–	62.34	–	-21.14
100	–	0.609	–	0.196	–	83.34	–	-33.06
150	–	0.611	–	0.187	–	103.12	–	-38.83
200	–	0.619	–	0.184	–	121.01	–	-46.66
250	–	0.620	–	0.179	–	123.67	–	-48.23
300	–	0.627	–	0.176	–	135.62	–	-53.86
				1				
5	0.843	–	–	–	1.68	–	–	–
10	0.867	–	–	–	2.59	–	–	–
25	0.859	–	–	–	4.92	–	–	–
50	0.866	–	–	–	5.85	–	–	–
100	0.877	–	–	–	9.87	–	–	–
150	0.888	–	–	–	15.21	–	–	–
200	0.895	–	–	–	20.44	–	–	–
250	0.896	–	–	–	27.92	–	–	–
300	0.869	–	–	–	34.02	–	–	–
				3				
5	0.565	–	0.232	–	16.04	–	-0.64	–
10	0.574	–	0.214	–	20.93	–	-3.09	–
25	0.587	–	0.200	–	28.09	–	-3.93	–
50	0.599	–	0.191	–	38.38	–	-8.94	–
100	0.614	–	0.180	–	54.34	–	-17.09	–
150	0.623	–	0.171	–	68.25	–	-21.80	–
200	0.632	–	0.167	–	72.40	–	-25.10	–
250	0.638	–	0.160	–	79.34	–	-26.83	–
300	0.657	–	0.160	–	96.19	–	-22.63	–
				4				
5	–	0.640	–	0.353	–	24.00	–	-18.42
10	–	0.638	–	0.353	–	31.13	–	-19.62
25	–	0.618	–	0.344	–	39.67	–	-26.41
50	–	0.597	–	0.333	–	54.09	–	-27.95
100	–	0.605	–	0.227	–	72.76	–	-22.24
150	–	0.611	–	0.215	–	78.45	–	-24.30
200	–	0.615	–	0.201	–	78.37	–	-25.36
250	0.169	0.623	–	0.190		89.54	–	-26.87
300	0.148	0.647	–	0.179		89.87	–	-18.96
				5				
5	0.698	–	–	–	1.58	–	–	–
10	0.729	–	–	–	2.55	–	–	–
25	0.719	–	–	–	4.89	–	–	–

50	0.704	–	–	–	6.19	–	–	–
100	0.676	–	–	–	7.48	–	–	–
150	0.670	–	–	–	8.71	–	–	–
200	0.676	–	–	–	8.62	–	–	–
250	0.705	–	–	–	11.5	–	–	–
300	0.726	–	–	–	28.25	–	–	–
				6				
5	0.548	0.694	0.487	0.636	3.63	1.62	-2.82	-1.85
10	0.546	0.697	0.487	0.636	4.81	2.14	-3.72	-3.11
25	0.544	0.703	0.483	0.632	7.36	3.28	-5.75	-5.02
50	0.544	0.707	0.480	0.627	9.50	3.77	-6.80	-6.77
100	0.544	0.719	0.476	0.622	12.92	4.69	-9.00	-8.78
150	0.545	0.734	0.473	0.620	15.58	5.40	-10.49	-10.45
200	0.547	0.745	0.471	0.616	17.85	6.31	-11.94	-10.77
250	0.548	0.758	0.469	0.614	19.92	7.30	-13.59	-10.94
300	0.554	0.779	0.467	0.612	21.00	9.41	-14.97	-10.03

UV-vis and ESI-MS Studies of DA Derivatives. The oxidative transformations of **DA** derivatives were evaluated and compared with those of **DA** employing UV-vis spectroscopy as well as ESI-MS. Three compounds were selected to compare their structural modifications (*i.e.*, oxidative transformations in the presence of Aβ, Cu(II), and Cu(II)-treated Aβ) with those of **DA**; (i) The compounds containing a catechol moiety (*i.e.*, **3** and **4**) were selected because of its irreversible oxidation waves; (ii) **2**, which indicated fully irreversible electron transfer processes, was chosen to compare the results with **DA**, **3**, and **4**. In UV-vis experiments (Figure 2.7), no significant optical changes were observed for **DA** derivatives in a buffered solution over 60 min (Figure 2.7a). When the compounds were incubated with Cu(II) for 60 min (Figure 2.7b), **3**, the compound characterized by substitution of the amino group in **DA**'s structure to a methylamino group, indicated similar optical bands to those of **DA**; The growth of new peaks at *ca*. 308 nm and 475 nm, associated with the transition of the chrome form, was observed.[24,25] On the other hand, **4** with a dimethyl amino moiety indicated a slight spectral shift from *ca*. 280 nm to 285 nm, presenting no cyclization. Upon incubation of these derivatives with $A\beta_{40}$ in the absence or presence of Cu(II) (Figure 2.7c and 2.7d), more distinguishable structural transformations were observed. In particular, the presence of both $A\beta_{40}$ and Cu(II) accelerated structural transformations of **3** and **4**. In the case of **3**, the peaks at *ca*. 308 nm and *ca.* 475 nm were intensively increased within 10 min. A spectral shift from 280 nm to 308 nm was shown from **4**, suggesting its transformation to semiquinone form (but not cyclization).[24] The addition of Cu(II), $A\beta_{40}$, and Cu(II)-treated $A\beta_{40}$ slightly increased the absorbance intensity of **2** with 3,4-dimethoxy and amino groups at *ca*. 280 nm; however, no spectral changes were further detected.

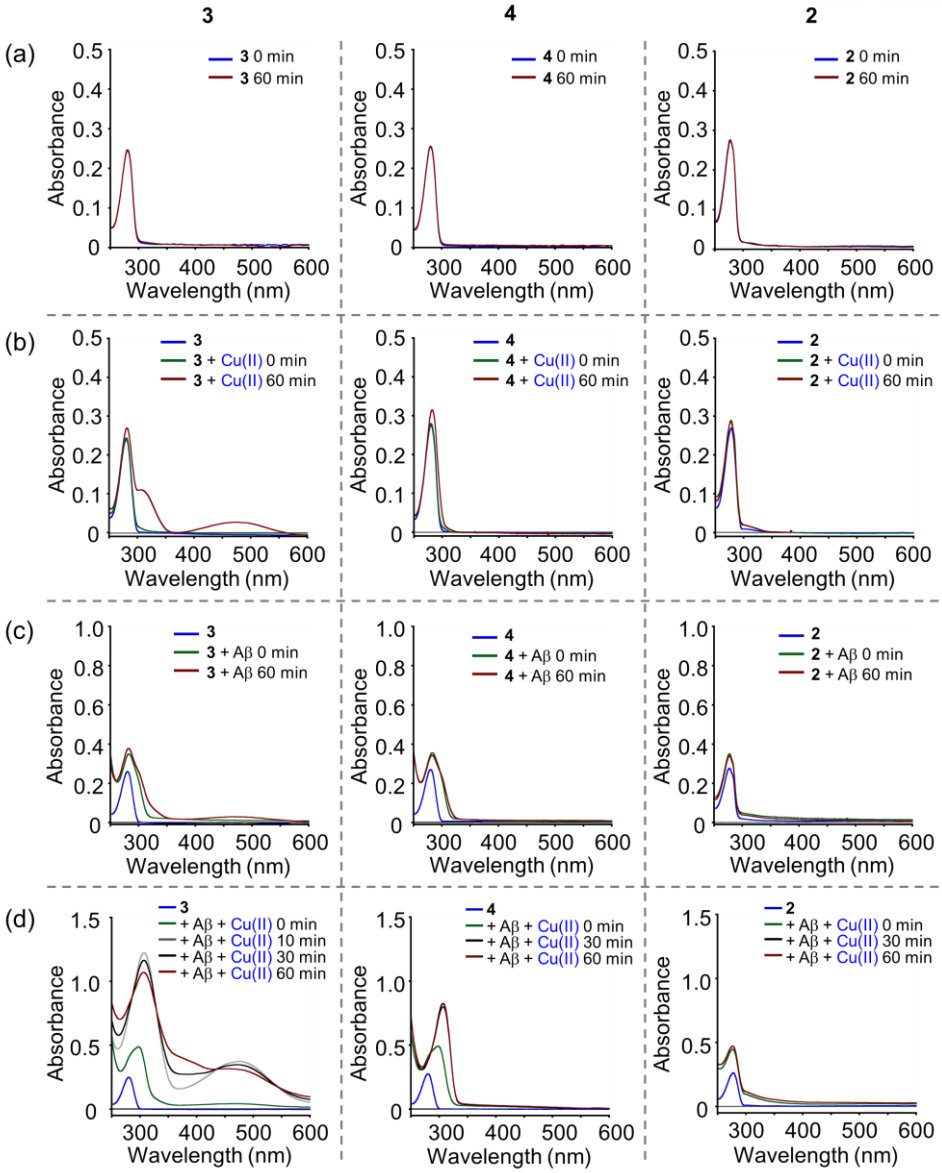

Figure 2.7. Transformations of **2**, **3**, and **4** with or without $CuCl_2$ and/or $A\beta_{40}$, monitored by UV-vis spectroscopy. UV-vis spectra of **2**, **3**, and **4** with or without $CuCl_2$ in the absence (a, b) or presence of $A\beta_{40}$ (c, d) were measured. Experimental conditions: [$A\beta_{40}$] = 50 μM; [$CuCl_2$] = 50 μM; [compound] = 100 μM, pH 6.6 (for Cu(II) samples) or pH 7.4 (for metal-free samples); 37 °C; 1 h incubation; no agitation.

Scheme 2.2. Proposed oxidative pathways of **DA** and its derivatives.

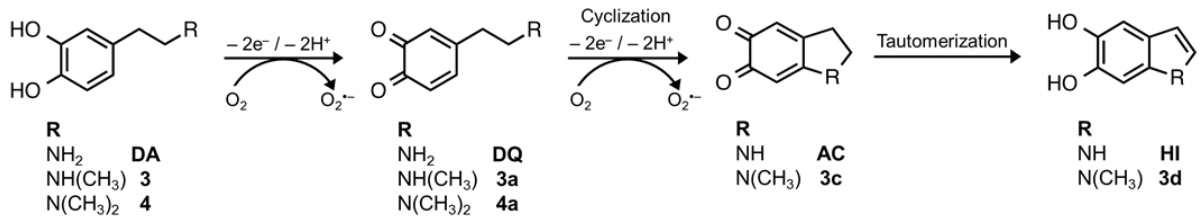

To identify the products from oxidation, the ESI-MS studies were conducted (Figure 2.8). The oxidative pathways of **3** and **4** were proposed (Scheme 2.2). Supporting the results obtained from UV-vis experiments, along with a peak at 168 *m/z* characterized by $[\mathbf{3} + H]^+$, the incubation of **3** with $A\beta_{40}$ and/or Cu(II) generated a 4 Da less new peak at 164 *m/z*, proposed to be a cyclized product of **3** (*e.g.,* **3c** or **3d**). The peaks corresponding to the cyclized form were not indicated from **4**; however, a peak at 180 *m/z* coincided with $[\mathbf{4a} + H]^+$ was observed by revealing its transition to the quinone form. Interestingly, in the presence of Cu(II)-treated $A\beta_{40}$, the peaks assigned to the transformed products were indicated from **3** and **4**, implicating their rapid oxidation. Comparing with **3** and **4**, the incubation of **2** with $A\beta_{40}$ and Cu(II)-treated $A\beta_{40}$ only showed a peak matched with $[\mathbf{2} + H]^+$. Overall, the importance of a catechol moiety on **DA**'s reactivity with Aβ, Cu(II), and Cu(II)-bound Aβ is reaffirmed. In addition, various oxidative transformations were observed by difference of the amino group in **DA** framework, possibly useful to further investigations to determination of how **DA**'s cyclization process could be associated with its regulatory activity toward metal-free Aβ and metal-induced Aβ aggregation.

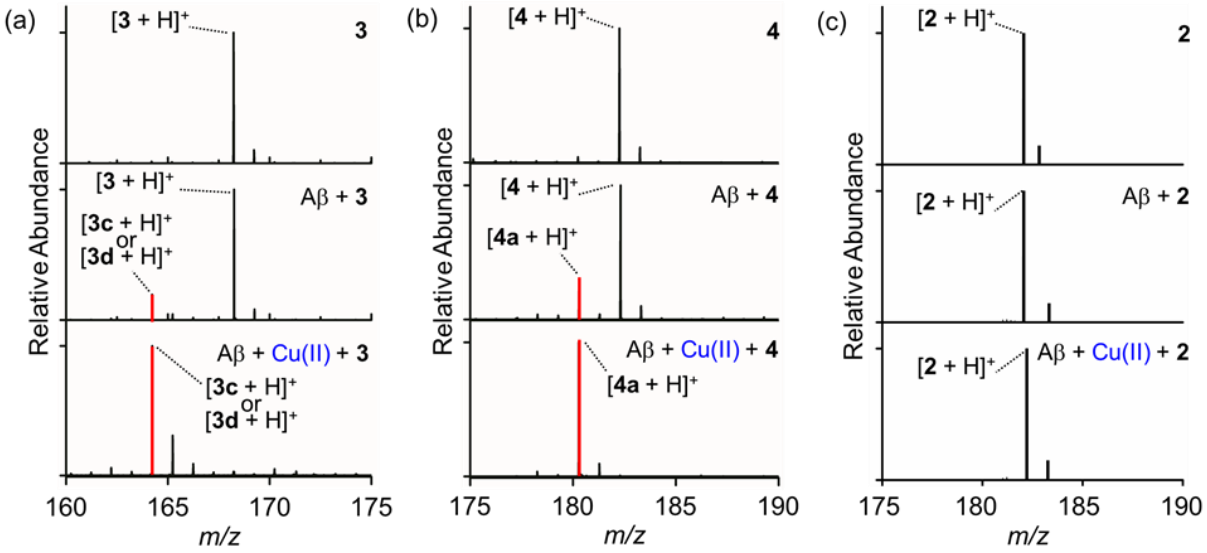

Figure 2.8. Transformation of **2**, **3**, and **4** with or without $CuCl_2$ and/or $A\beta_{40}$, monitored by mass spectrometry. Experimental conditions: $[A\beta_{40}]$ = 100 μM; $[CuCl_2]$ = 100 μM; [compound] = 500 μM; 100 mM ammonium acetate; pH 7.5; 37 °C; 1 h incubation; no agitation. The incubated samples were diluted by 10-fold before injection into the mass spectrometer.

Reactivity of DA Derivatives toward Metal-free and Metal-induced Aβ Aggregation. The reactivity of **DA** derivatives toward metal-free and metal-mediated Aβ aggregation was identified. In inhibition experiments (Figure 2.9), the compounds, which indicated their redox-active properties and oxidative transformations, were able to modulate metal-free and Cu(II)-bound Aβ aggregation pathways.

Discernible smearing bands were not observed when Aβ was incubated with **1**, **2**, and **5**. Although **6** showed its potential oxidation based on lower i_{pa}, in the CV studies, it did not affect Aβ aggregation. **3**, the compound showing its cyclized products, modulated the MW of both metal-free $A\beta_{40/42}$ and Cu(II)-bound $A\beta_{40/42}$ generating amorphous aggregates, observed by TEM. On the other hand, **4**, the compound showing only quinone products from its oxidative transformation, could control the aggregation of Cu(II)-bound Aβ (but not metal-free Aβ). Fibrillar $A\beta_{42}$ was identified when $A\beta_{42}$ was incubated with **4** in the absence of Cu(II) (the data is not shown); however, the addition of Cu(II) to the **4**-treated $A\beta_{42}$ sample showed smaller and unstructured aggregates.

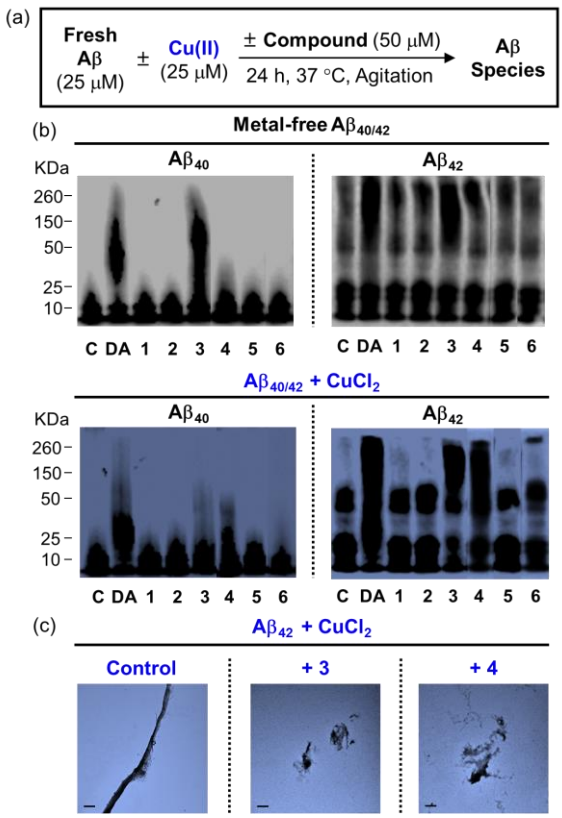

Figure 2.9. Capacity of **DA** derivatives to control metal-free and metal-induced Aβ aggregation. (a) Scheme of inhibition experiments. (b) Visualization of the size distribution of the resultant Aβ species in the absence or presence of **DA** derivatives (c) TEM images of the resultant metal-free and metal-induced Aβ aggregates from the 24 h incubated samples. The scale bar is 500 nm. Experimental conditions: [$A\beta_{40}$ or $A\beta_{42}$] = 25 μM; [$CuCl_2$] = 25 μM; [compound] = 50 μM; pH 6.6 (for Cu(II) samples) or pH 7.4 (for metal-free samples); 37 °C; 24 h incubation; constant agitation.

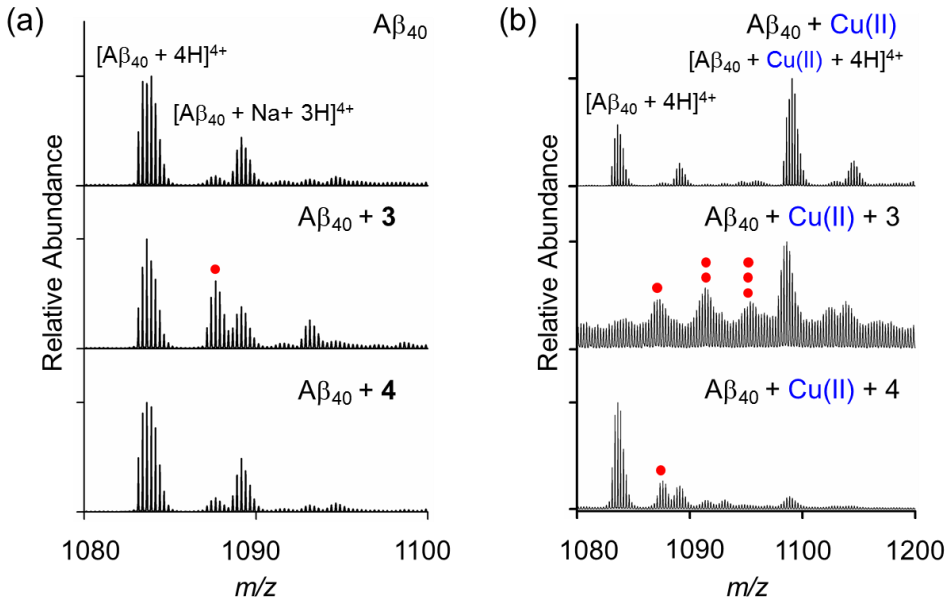

Figure 2.10. Mass spectrometric analyses of $A\beta_{40}$ monomers treated with **3** and **4** in the absence or presence of Cu(II). The addition of an oxygen atom is marked in a red dot. Experimental conditions: $[A\beta_{40}]$ = 100 μM; $[CuCl_2]$ = 100 μM; [compound] = 500 μM; pH 7.5; 37 °C; 6 h incubation (for metal-free samples) or 1 h incubation (for Cu(II) samples); 100 mM ammonium acetate. The incubated samples were diluted by 10-fold before injection into the mass spectrometer.

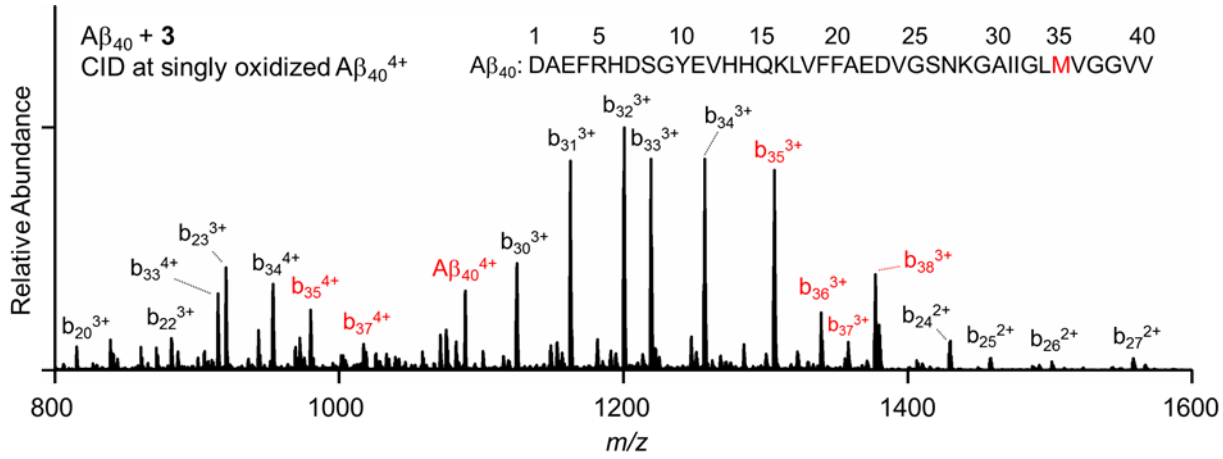

Figure 2.11. MS/MS sequencing of the oxidized $A\beta_{40}^{4+}$ peak $[A\beta_{40} + O + 4H]^{4+}$. Experimental conditions: $[A\beta_{40}]$ = 100 μM; [compound] = 500 μM; pH 7.5; 37 °C; 6 h incubation; 100 mM ammonium acetate. The incubated samples were diluted by 10-fold before injection into the mass spectrometer.

ESI-MS studies showed that the reactivities of **3** and **4** toward metal-free and Cu(II)-mediated $A\beta_{40}$ aggregation were also associated with peptide oxidation (Figure 2.10; maked in red dots). Aβ incubated with **3** indicated the peaks corresponding to an oxygen atom added to $A\beta_{40}^{4+}$ monomer; more oxidation of Aβ was observed in the presence of Cu(II). MS/MS data identified that an oxygen

atom was bound to the Met35 residue of metal-free $A\beta_{40}^{4+}$ monomer, which was consistent with the studies using **DA** (Figure 2.11). In addition, the MS data suggested the oxidation of $A\beta_{40}$ incubated with **4** in the presence of Cu(II), which could be analyzed regarding the results obtained from gel/Western blot and TEM studies.

2.3. Conclusion

DA is suggested to be linked to the pathological components found in AD; however, it is unclear how it could interact or react with them at the molecular level. In our present studies, the interactions of **DA** with metal-free Aβ, metals, metal-bound Aβ, and ROS, known to the pathological agents in AD, were observed. The different reactivity of **DA** toward metal-free Aβ and metal-bound Aβ under aerobic and anaerobic conditions was indicated. Under our experimental conditions for ESI-MS, IM-MS, and MS/MS, the reactivity of **DA** toward metal-free and metal-bound Aβ aggregation was linked to Aβ oxidation by **DA**. In particular, the oxidation of Met35 in Aβ, which could impede Aβ aggregation, was presented when **DA** was incubated with metal-free Aβ. Furthermore, our structure-reactivity investigations have presented that the overall oxidative transformations of **DA** would be important for altering metal-free and metal-bound Aβ aggregation pathways. Overall, our multidisciplinary investigations demosntrate **DA**'s mode of action toward multiple pathogenic features in AD.

2.4. Experimental Section

Materials and Methods

All reagents were purchased from commercial suppliers and used as received unless otherwise stated. **3** was prepared following a previously reported method.[26] **DA**, **1**, **2**, and **5** were purchased from Sigma (St. Louis, MO, USA); **4** and **6** were acquired from Enamine (Monmouth Junction, NJ, USA). Trace metal contamination was removed from buffers and solutions used for Aβ experiments by treating with Chelex (Sigma) overnight. $A\beta_{40}$ (DAEFRHDSGYEVHHQKLVFFAEDVGSNKGAIIGLMVGG-VV) and $A\beta_{42}$ (DAEFRHDSGYEVHHQKLVFFAEDVGSNKGAIIGLMVGGVVIA) were purchased from Anaspec (Fremont, CA, USA) and Anygen (Nam-myun, Jangseong-gun, Republic of Korea). Double distilled H_2O (ddH_2O) was obtained from a Milli-Q Direct 16 system (Merck KGaA, Darmstadt, Germany). Anaerobic reactions were performed in a N_2-filled glovebox (Korea Kiyon, Bucheon-si, Gyeonggi-do, Republic of Korea). Optical spectra were recorded on an Agilent 8453 UV-vis spectrophotometer. Mass spectrometric analyses were carried out using a Synapt G2-Si quadrupole time-of-flight mass spectrometer (Waters, Manchester, UK) or High Capacity Ion Trap (HCT) mass spectrometer (Bruker Daltonics, Billerica, MA, USA). Transmission electron microscopy (TEM) images were collected on a JEOL JEM-2100 transmission electron microscope (UNIST Central

Research Facilities, Ulsan, Republic of Korea).

Electrochemistry

Cyclic voltammograms were recorded under N_2 (g) with a CHI620E model potentiostat (Qrins, Seoul, Republic of Korea). A three-electrode setup was utilized, consisting of an Ag/AgCl reference electrode (RE-1B Reference electrode (Ag/AgCl); Qrins, Seoul, Republic of Korea), a Pt wire auxiliary electrode (SPTE Platinum electrode; Qrins, Seoul, Republic of Korea), and a glassy carbon working electrode (Qrins, Seoul, Republic of Korea). Electrochemical analysis of **DA** and its structural derivatives (**1** and **3-6**; 1 mM) were recorded in H_2O with 1 M NaCl as a supporting electrolyte at scan rates of 5, 10, 25, 50, 100, 150, 200, 250, and 300 mV/s at room temperature.

Spectroelectrochemistry

Spectroelectrochemical results for **DA** was recorded under N_2 (g) with a CHI620E model potentiostat (Qrins, Seoul, Republic of Korea). Optical spectra were recorded on an Agilent 8453 UV-vis spectrophotometer. A spectroelectrochemical cell kit was utilized containing a thin layer quartz glass cell, a Pt gauze working electrode, a Pt wire auxiliary electrode (SEC-C Spectroelectrochemical cell kit (Pt); Qrins, Seoul, Republic of Korea), and an Ag/AgCl reference electrode (RE-1B Reference electrode (Ag/AgCl); Qrins, Seoul, Republic of Korea). Optical spectra of **DA** were monitored at potentials of 0.627 V in H_2O with 1 M NaCl as a supporting electrolyte at 37 °C over 60 min.

Amyloid-β Preparation

Aβ peptides were dissolved in ammonium hydroxide (NH_4OH, 1% v/v, aq), aliquoted, lyophilized, and stored at −80 °C. A stock solution (*ca*. 150 μM) was prepared by re-dissolving Aβ with NH_4OH (1% w/v, aq., 10 μL) followed by dilution with H_2O. The concentration of the solution was determined by measuring the absorbance of the solution at 280 nm (ε = 1450 $M^{-1}cm^{-1}$ for $A\beta_{40}$; ε = 1490 $M^{-1}cm^{-1}$ for $A\beta_{42}$).

Transformations of Compounds Detected by UV-vis Spectroscopy

Optical spectra of **DA** and its structural analogues (**2-4**; 100 μM) with or without $CuCl_2$ (50 μM) in the absence or presence of $A\beta_{40}$ (50 μM) were recorded on an Agilent 8453 UV-vis spectrophotometer. Chelex-treated buffered solutions including HEPES [20 μM, pH 6.6 (for Cu(II) samples) or 7.4 (for metal-free and Zn(II) samples), and 150 μM NaCl] were used for the experiment.

Electrospray Ionization Mass Spectrometry (ESI-MS) and Tandem MS (MS/MS)

ESI-MS spectra of **DA**, **3**, and **4** were recorded using a Synapt G2-Si quadrupole time-of-flight mass

spectrometer (Waters, Manchester, UK) equipped with electrospray ionization source. The spectra of **2** were obtained using a High Capacity Ion Trap (HCT) mass spectrometer (Bruker Daltonics, Billerica, MA, USA). For ESI-MS, the capillary voltage, sampling cone voltage, and source temperature were adjusted to 2.8 kV, 70 V, and 40 °C. Tandem MS experiments were conducted for the +4-charged singly oxidized $A\beta_{40}$ with 1087.1 *m/z* (monoisotopic mass 1086.6 *m/z*) by setting the trap collision energy, LM resolution, and HM resolution as 55 eV, 10, and 15, respectively. All mass spectra were obtained under the IMS mode to measure the drift time for each ion. Trap gas flow (Ar), helium gas flow, and IMS gas flow (N_2) were set as 4 mL/min, 120 mL/min, and 30 mL/min, respectively. IMS wave velocity and wave height were adjusted to 450 m/s and 10 V. To investigate the transformation of **DA** and its structural derivatives (**2**-**4**), **DA** and its structural analogues (**2**-**4**) (500 μM) were incubated with or without $A\beta_{40}$ (100 μM) in 100 mM ammonium acetate, pH 7.5, in the absence or presence of $CuCl_2$ (100 μM). The samples were incubated at 37 °C for 1 h. To further probe the influence of **DA** and its structural derivatives (**3** and **4**) on $A\beta_{40}$ aggregation, samples in the presence of $A\beta_{40}$ were prepared following the methods. Metal-free and $CuCl_2$-treated samples were incubated at 37 °C for 8 h and 1 h, respectively. The incubated samples were diluted by 10-fold before injection into the mass spectrometer.

Aβ Aggregation Experiments

All experiments were conducted according to previously published methods.[19] The peptide stock solution was diluted to a final concentration of 25 μM in the Chelex-treated buffered solution containing HEPES [20 μM; pH 7.4 (for metal-free and Zn(II) samples) or pH 6.6 (for Cu(II) samples), and NaCl (150 μM)]. For inhibition experiments, Aβ (25 μM) was first treated with or without a metal chloride salt ($CuCl_2$ or $ZnCl_2$; 25μM) for 2 min followed by addition of compounds (50 μM; 1% v/v final DMSO concentration). The resulting samples were incubated at 37 °C for 24 h with constant agitation. For disaggregation experiments, Aβ in the absence or presence of a metal chloride salt ($CuCl_2$ or $ZnCl_2$) was initially incubated at 37 °C for 24 h with constant agitation. The compound was added into the resulting solution afterward followed by an additional 24 h of incubation at 37 °C with constant agitation. For anaerobic conditions, all samples were prepared in an N_2-filled glovebox.

Gel Electrophoresis with Western Blotting

The samples from inhibition and disaggregation experiments were analyzed by gel electrophoresis with Western blotting (gel/Western blot) using an anti-Aβ antibody (6E10). Each sample (10 μL) was separated on a 10−20% Tris-tricine gel (Invitrogen, Grand Island, NY, USA). Following separation, the proteins were transferred onto nitrocellulose, which was blocked with bovine serum albumin

(BSA, 3% w/v, RMBIO, Missoula, MT, USA) in Tris-buffered saline (TBS) containing 0.1% Tween-20 (TBS-T) for 4 h at room temperature. The membranes were incubated with antibody (6E10, 1:2000, Covance, Princeton, NJ, USA) in a solution of 2% BSA (w/v in TBS-T) for 4 h at room temperature or overnight at 4 °C. After washing, the horseradish peroxidase-conjugated goat anti-mouse secondary antibody (1:5000) in 2% BSA was added for 1 h at room temperature. Biosesang ECL Plus kit (Biosesang, Gyeonggi-do, Republic of Korea), or a homemade ECL kit was used[27] to visualize the results on a ChemiDoc MP Imaging System (BioRad, Hercules, CA, USA).

Transmission Electron Microscopy (TEM)

Samples for TEM were prepared according to previously reported methods.[20] Glow-discharged grids (Formar/Carbon 300-mesh, Electron Microscopy Sciences, Hatfield, PA, USA) were treated with Aβ samples from inhibition and disaggregation experiments (5 μL) for 2 min at room temperature. Excess sample was removed using filter paper followed by washing three times with H_2O. Each grid was incubated with uranyl acetate (1% w/v H_2O, 5 μL, 1 min). Upon removal of excess uranyl acetate with filter paper, the grids were dried for at least 30 min at room temperature before measurement. Images from each sample were taken on a JEOL JEM-2100 transmission electron microscope (UNIST Central Research Facilities, UNIST, Ulsan, Republic of Korea) at 120 kV and 25000× magnification.

2.5. Acknowledgments

This work was supported by the National Research Foundation of Korea (NRF) Grant funded by the Korean Government (NRF-2014R1A2A2A01004877 and NRF-2014S1A2A2028270) (to M.H.L.).

2.6. References

1. J. I. Rossato, L. R. M. Bevilaqua, I. Izquierdo, J. H. Medina and M. Cammarota, *Science*, 2009, **325**, 1017-1020.
2. J. Segura-Aguilar, I. Paris, P. Muñoz, E. Ferrari, L. Zecca and F. A. Zucca, *J. Neurochem*, 2014, **129**, 898-915.
3. M. Bisaglia, S. Mammi and L. Bubacco, *J. Biol. Chem.*, 2007, **282**, 15597-15605.
4. W. Linert, E. Herlinger, R. F. Jameson, E. Kienzl, K. Jellinger and M. B. Youdim, *Biochim. Biophys. Acta* 1996, **1316**, 160-168.
5. L. Zecca, L. Casella, A. Albertini, C. Bellei, F. A. Zucca, M. Engelen, A. Zadlo, G. Szewczyk, M. Zareba and T. Sarna, *J. Neurochem*, 2008, **106**, 1866-1875.
6. L. Zecca, C. Bellei, P. Costi, A. Albertini, E. Monzani, L. Casella, M. Gallorini, L. Bergamaschi, A. Moscatelli, N. J. Turro, M. Eisner, P. R. Crippa, S. Ito, K. Wakamatsu, W. D. Bush, W. C. Ward, J. D. Simon and F. A. Zucca, *Proc. Natl. Acad. Sci. U.S.A.*, 2008, **105**,

17567-17572.

7. J. Li, M. Zhu, A. B. Manning-Bog, D. A. Di Monte and A. L. Fink, *FASEB J.*, 2004, **18**, 962-964.
8. A. S. DeToma, S. Salamekh, A. Ramamoorthy and M. H. Lim, *Chem. Soc. Rev.*, 2012, **41**, 608-621.
9. S. E. Perez, O. Lazarov, J. B. Koprich, E.-Y. Chen, V. Rodriguez-Menendez, J. W. Lipton, S. S. Sisodia and E. J. Mufson, *J. Neurosci.*, 2005, **25**, 10220-10229.
10. I. Paris, A. Dagnino-Subiabre, K. Marcelain, L. B. Bennett, P. Caviedes, R. Caviedes, C. O. Azar and J. Segura-Aguilar, *J. Neurochem.*, 2001, **77**, 519-529.
11. T. Kawashima, K. Ohkubo and S. Fukuzumi, *J. Phys. Chem. B,* 2010, **114**, 675-680.
12. C. Opazo, X. Huang, R. A. Cherny, R. D. Moir, A. E. Roher, A. R. White, R. Cappai, C. L. Masters, R. E. Tanzi, N. C. Inestrosa and A. I. Bush, *J. Biol. Chem.*, 2002, **277**, 40302-40308.
13. S. L. Leong, C. L. L. Pham, D. Galatis, M. T. Fodero-Tavoletti, K. Perez, A. F. Hill, C. L. Masters, F. E. Ali, K. J. Barnham, R. Cappai, *Free Rad. Bio. Med.,* 2009, **46**, 1328-1337.
14. L. Hou, I. Kang, R. E. Marchant and M. G. Zagorski, *J. Biol. Chem.*, 2002, **277**, 40173-40176.
15. M. Palmblad, A. Westlind-Danielsson and J. Bergquist, *J. Biol. Chem.*, 2002, **277**, 19506-19510.
16. G. Bitan, B. Tarus, S. S. Vollers, H. A. Lashuel, M. M. Condron, J. E. Straub and D. B. Teplow, *J. Am. Chem. Soc.*, 2003, **125**, 15359-15365.
17. D. A. Butterfield and R. Sultana, *J. Amino Acids*, 2011, **2011**, 10.
18. Michele F. M. Sciacca, Samuel A. Kotler, Jeffrey R. Brender, J. Chen, D.-k. Lee and A. Ramamoorthy, *Biophys. J.*, 2012, **103**, 702-710.
19. A. Quist, I. Doudevski, H. Lin, R. Azimova, D. Ng, B. Frangione, B. Kagan, J. Ghiso and R. Lal, *Proc. Natl. Acad. Sci. U.S.A.,* 2005, **102**, 10427-10432.
20. J. S. Derrick, R. A. Kerr, Y. Nam, S. B. Oh, H. J. Lee, K. G. Earnest, N. Suh, K. L. Peck, M. Ozbil, K. J. Korshavn, A. Ramamoorthy, R. Prabhakar, E. J. Merino, J. Shearer, J.-Y. Lee, B. T. Ruotolo and M. H. Lim, *J. Am. Chem. Soc.*, 2015, **137**, 14785-14797.
21. J. Bieschke, J. Russ, R. P. Friedrich, D. E. Ehrnhoefer, H. Wobst, K. Neugebauer and E. E. Wanker, *Proc. Natl. Acad. Sci. U.S.A.,* 2010, **107**, 7710-7715.
22. S. I. A. Cohen, S. Linse, L. M. Luheshi, E. Hellstrand, D. A. White, L. Rajah, D. E. Otzen, M. Vendruscolo, C. M. Dobson and T. P. J. Knowles, *Proc. Natl. Acad. Sci. U.S.A.,* 2013, **110**, 9758-9763.
23. D. G. Graham, *Mol. Pharmacol.*, 1978, **14**, 633-643.
24. W. J. Barreto, S. R. G. Barreto, R. A. Ando, P. S. Santos, E. DiMauro and T. Jorge, *Spectrochim. Acta. A Mol. Biomol. Spectrosc.*, 2008, **71**, 1419-1424.
25. W. J. Barreto, S. Ponzoni and P. Sassi, *Spectrochim. Acta. A Mol. Biomol. Spectrosc.*, 1998,

55, 65-72.

26. R. J. Borgman, J. J. McPhillips, R. E. Stitzel, I. J. Goodman, *J. Med. Chem.,* 1973, ***16***, 630-633.

27. D. D. Mruk, C. Y. Cheng, *Spermatogenesis,* 2011, **1**, 121-122.

Chapter 3.

Detection of Metal Ions by Fluorescent Probes in Living Cells

The results presented in this chapter have been published; (1) Choi, Y. W.; Lee, J. J.; Nam, E.; Lim, M. H.; Kim .C., *Tetrahedron.*, 2016, **72**, 1998-2005; (2) Lee, J. J.; Kim, Y. S.; Nam, E.; Lee, S. Y.; Lim, M. H.; Kim. C., *Dalton Trans.*, 2016, **45**, 5700-5712; (3) Jo, T, G. ; Lee, J. J., Nam, E. ; Bok, K. H. ; Lim, M. H. ; Kim, C., *New J. Chem.*, 2016, **40**, 8918-8927. I conducted imaging experiment to monitor fluorescent responses of newly developed sensors to metal ions in living cells.

3.1. Introduction

Metals in the brain (*e.g.,* copper, zinc, iron) are involved in signaling pathways and receptor's and transporters' functions (*e.g.*, NMDAR, ATP7A);[1,2] however, they are strictly regulated since metal ion dyshomeostasis, one of the symptoms in AD, could occur the elevation of oxidative stress and dysfunction of metalloproteins essential for biological fucntions. Moreover, the accumulation of toxic heavy metals, such as mercury, in neuromelanin pigments affects degeneration of neurons.[3,4] Multiple methods have been developed to visualize actions of metals in the brain. One of the methods applied to observe metals' actions is fluorescence imaging using chemical fluorescent probes in conjunction with fluorescence microscopy. Selective and sensitive fluorescent sensors for specific metal ions have advanced the visualization of metals' functions.[5] Herein, our studies demonstrate the design of newly developed sensor for metal ions and their fluorescent responses to metal ions in living cells.

3.2. Results and Discussion

3.2.1. Fluorescenct Responses of Compound A to Al(III) in Living Cells

Scheme 3.1. Proposed binding mode of Al(III)−**A**.

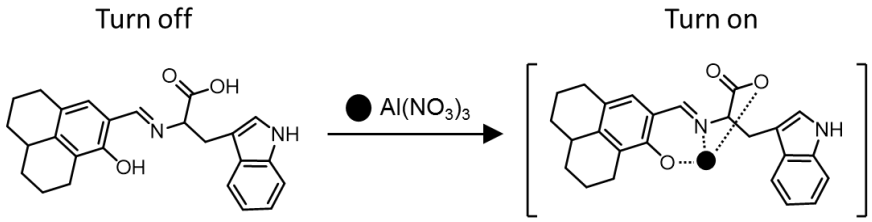

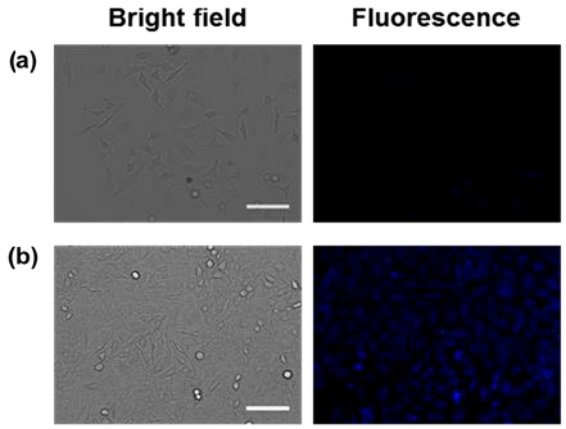

Figure 3.1. Fluorescent responses of **A** to Al(III) in HeLa cells. Cells were exposed to (a) 0 and (b) 300 μM Al(III) for 4 h prior to addition of **A** (10 μM). Experimental conditions: 37 °C; 5% CO_2. The scale bar is 100 μm. The DAPI light cube [DAPI, 2-(4-Amidinophenyl)-1*H*-indole-6-carboxamidine; excitation 357 (± 22) nm; emission 447 (± 30) nm] was employed to perform imaging experiments.

The compound **A** was developed based on a linkage of julolidine and tryptophan moiety due to julolidines' good applicability in aqueous solution and tryptophan's fluorescence property, along with noncovalent binding forces between metal ions and its indole ring.[6,7] The designed and synthesized sensor **A** appeared fluorescent responses in the presence of Al(III). Herein, we report the fluorescent response of **A** to Al(III) in living cells (Figure 3.1). HeLa cells were exposed to **A** (10 μM) after preincubation with Al(III) (300 μM) for 4 h. **A** revealed its fluorescent response to Al(III) at DAPI channel [excitation 357 (± 22) nm; emission 447 (± 30) nm], while discernible fluorescence did not occur from living cells with either Al(III) or **A**. Therefore, the potential ability of the new fluorescent probe **A** in biological systems was indicated.

3.2.2. Fluorescent Responses of Compound B to Hg(II) in Living Cells

Scheme 3.2. Fluorescent enhancement mechanism and proposed binding mode of Hg(II)–**B** .

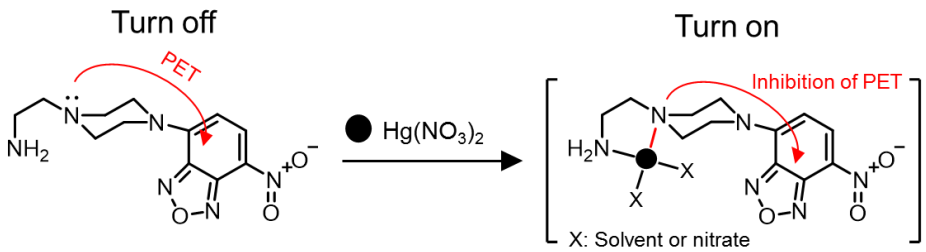

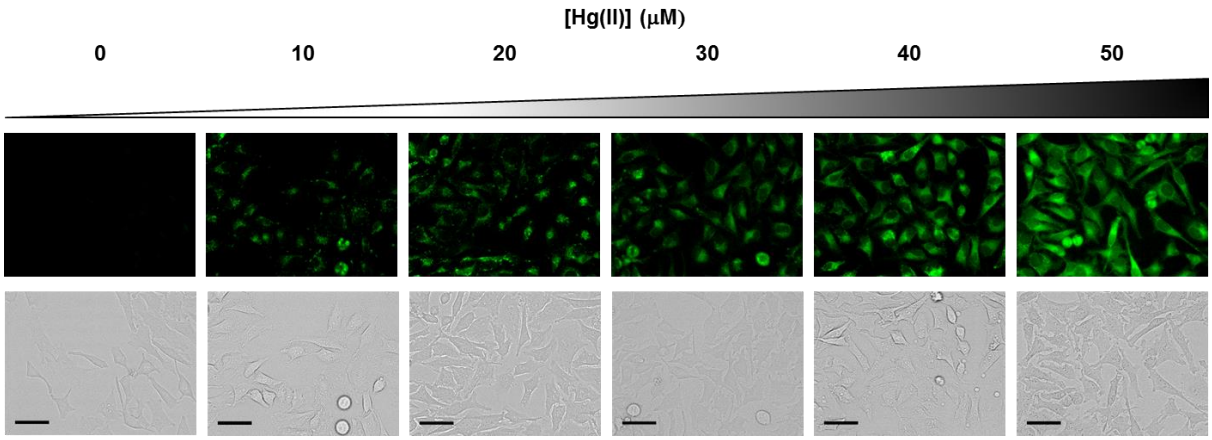

Figure 3.2. Fluorescent responses of **B** to Hg(II) in HeLa cells. Cells were pre-incubated with **B** for 5 min prior to addition of various concentrations of Hg(II). Experimental conditions: [Hg(II)] = 0, 10, 20, 30, 40, and 50 μM; [**B**] = 5 μM; 37 °C; 5% CO_2. The scale bar is 50 μm. The GFP light cube [excitation 470 (±11) nm; emission 510 (±21) nm] was used to detect the fluorescence.

The sensor, **B**, for detecting Hg(II), was synthesized and developed based on the photoinduced

electron transfer (PET) principle.[8] To investigate the fluorescent responses of **B** to Hg(II) in living HeLa cells, imaging experiments were carried out (Figure 3.2). Various concentrations of Hg(II) (*i.e.*, 0, 10, 20, 30, 40, and 50 μM) were treated to the cells before treatment of **B**. The fluorescent responses of **B** to Hg(II) were observed in a concentration-dependent manner. Any noticeable fluorescent response was not observed from the cells incubated with either Hg(II) or **B**. Thus, these results confirmed that **B** could be a potential chemosensor to detect Hg(II) in biological systems.

3.2.3. Fluorescent Responses of Compound C to Al(III) in Living Cells.

Scheme 3.3. Fluorescent enhancement mechanism and proposed binding mode of Al(III)–**C**.

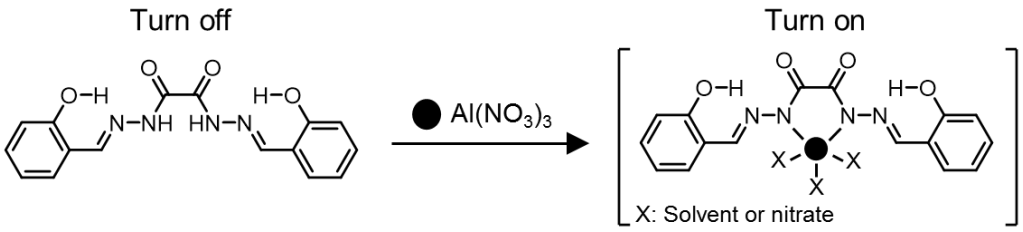

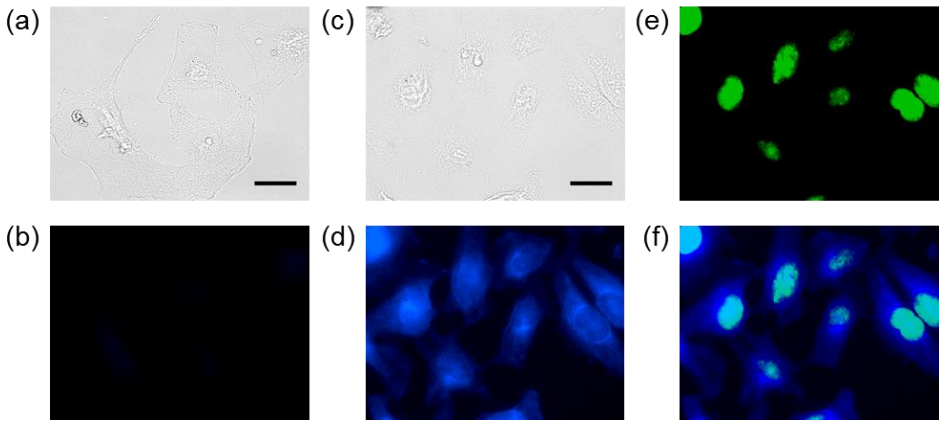

Figure 3.3. Fluorescent responses of **C** to Al(III) in HeLa cells. Cells were exposed to (a and b) 0 or (c-f) 100 μM Al(III) for 1 h prior to addition of **C** (20 μM). (a and c) Bright-field images of cells without or with Al(III), respectively. Fluorescent responses to Al(III) were detected in the (b) absence or (d) presence of Al(III). To investigate the distribution of fluorescence, (e) the nuclei of cells were stained with **SYTO16** (2.5 μM). (f) Overlapped fluorescence images of (d) and (e). Experimental conditions: DAPI channel [λ_{ex} = 357 (± 22) nm; λ_{em} = 447 (± 30) nm] for (b) and (d); GFP channel [excitation 470 (±11) nm; emission 510 (±21) nm] for (e). The scale bar is 25 μm.

The sensor **C**, for Al(III) in aqueous solution, was developed through the combination of 2-hydroxybenzaldehyde and oxalohydrazide. To examine the fluorescent responses of **C** to Al(III) in biological systems, imaging experiments were conducted using HeLa cells (Figure 3.3). Fluorescent responses of **C** for Al(III) were only indicated in the presence of Al(III) (Figure 3.3d). To identify the

fluorescent localization in the cells, the nuclei were stained with **SYTO16** (Figure 3.3e). As shown in Figure 3.3f, the overlapped fluorescent image between **C** with Al(III) and **SYTO16**, the fluorescent dye for the nuclei, suggests that the probe's fluorescent response to Al(III) occur in the overall parts of cells, including nuclei and cytoplasms. Our results suggest the potential use of **C** as a metal sensor in biological systems.

3.3. Conclusion

Diverse metal ions are vital targets to be detected in order to understand their important roles (*e.g.*, signaling, neurotoxicity) in normal and disease-affected brains. Thus, sensitive and selective fluorescent sensors have been developed to visualize the localization and actions of metal ions. The newly developed sensors, described from our studies, **A**, **B**, and **C**, are shown to indicate their fluorescent response to specific metal ions [*i.e.*, Al(III) for **A** and **C**, Hg(II) for **B]** in living cells. In the near future, further modifications of these probes should be carried out to improve their properties, including biocompatibility and specificity for metal ions.

3.4. Experimental Section

Imaging Experiments

HeLa cells were maintained in media containing DMEM, 10% fetal bovine serum (FBS, GIBCO, Grand Island, NY, USA), 100 U/mL penicillin (GIBCO), and 100 mg/mL streptomycin (GIBCO). The cells were grown in a humidified atmosphere with 5 % CO_2 at 37 °C. Cells were seeded onto imaging dish (SPL Life Sciences Co., Ltd., South Korea) at a density of 150,000 cells per 1 mL and then incubated at 37 °C for 24 h. Cells were treated with various concentration of metal ions (dissolved in water) and compounds (dissolved in DMSO; 1% v/v final DMSO concentration; at room temperature). Cells were washed with 10 mM bis-Tris buffer (pH 7.4, 150 mM NaCl) twice. Imaging experiments were performed with an EVOS FL fluorescence microscope (Life technologies) using a DAPI light cube [DAPI, 2-(4-Amidinophenyl)-1H-indole-6-carboxamidine; excitation 357 (± 22) nm; emission 447 (± 30) nm] or GFP light cube [excitation 470 (± 11) nm; emission 510 (± 21) nm].

3.5. Acknowledgments

This work was supported by the National Research Foundation of Korea (NRF) Grant funded by the Korean Government [NRF-2014R1A2A2A01004877 and NRF-2014S1A2A2028270 to M.H.L.]

3.6. References

1. A. I. Bush and R. E. Tanzi, *Neurotherapeutics*, 2008, **5**, 421-432.
2. M. G. Savelieff, S. Lee, Y. Liu and M. H. Lim, *ACS Chem. Biol.*, 2013, **8**, 856-865.
3. L. Zecca, C. Bellei, P. Costi, A. Albertini, E. Monzani, L. Casella, M. Gallorini, L.

Bergamaschi, A. Moscatelli, N. J. Turro, M. Eisner, P. R. Crippa, S. Ito, K. Wakamatsu, W. D. Bush, W. C. Ward, J. D. Simon and F. A. Zucca, *Proc. Natl. Acad. Sci. U.S.A.,* 2008, **105**, 17567-17572.

4. J. Segura-Aguilar, I. Paris, P. Muñoz, E. Ferrari, L. Zecca and F. A. Zucca, *J. Neurochem.*, 2014, **129**, 898-915.
5. K. P. Carter, A. M. Young and A. E. Palmer, *Chem. Rev.*, 2014, **114**, 4564-4601.
6. J. Y. Noh, S. Kim, I. H. Hwang, G.Y. Lee, J. Kang, S.H. Kim, J. Min, S. Park, C. Kim, J. Kim, *Dyes Pigm.,* 2013, **99**, 1016-1021.
7. S.L. de Wall, E.S. Meadows, L.J. Barbour, G.W. Gokel, *J. Am. Chem. Soc*., 1999, **121**, 5613-5614.
8. M. Choi, M. Kim, K. D. Lee, K.-N. Han, I.-A. Yoon, H.-J. Chung and J. Yoon, *Org. Lett*., 2001, **3**, 3455-3457.

Acknowledgments

Completion of this thesis was impossible without the support of many people. I would like to express my sincere gratitude to all of them.

Foremost, I would like to thank my supervisor, Prof. Mi Hee Lim, for the continuous support of my studies. She has always cared about our group members with sincere guidance. Her advice has helped me in all time of research and writing of review / research articles, and thesis. When I first entered the Lim lab, many things were not familiar with me. It took more time to comprehend knowledges for experiments and studies; however, she always led me with insightful directions and answered my questions in spite of her busy schedules. Without her motivation, patience, suggestion, knowledge and kind teaching, I could not finish my my master's degree. It would be hard to describe my all of my appreciation for her.

I would like to thank the members of my committee, Professor Hyun-woo Rhee and Professor Jung-Min Kee for sparing their precious time to read my thesis and providing invaluable advice despite their busy schedules.

I want to thank all of my current Lim lab group members, Hyuck Jin Lee, Shin Jung Lee, Juhye Kang, Kyle Korshavn, Yonghwan Ji, Jiyeon Han, Suwon Lee, Misun Lee, Jong-Min Suh, Geewoo Nam, Mingeun Kim, Yelim Yi, Nahye Park, Donghyeon Kim, and our previous group member, Jeffrey S. Derrick, for their assistance and cooperation. I also want to thank Mi Sook Lim, our group manager, for her encouragement and kind guidance for our lab. They always gave me positive energy and scientific motivation. I cannot imagine my graduate school years without them. It has been my great pleasure to work with you all. In addition, I have been very grateful to the people whom I have collaborated with. They have been always helpful and have given me scientific knowledge which that I did not have before.

Lastly, I would like to thank my father (In Tae Nam), my mother (Myung Sun Yoon), and my sister (Min Joo Nam) for their great support and encouragement.

Eunju Nam

Department of Chemistry
Ulsan National Institute of Science and Technology (UNIST)
Ulsan 44919, Republic of Korea
Email: n3329@unist.ac.kr

Education

Mar. 2015 – Feb. 2017 **M.S., Chemistry, UNIST**, Ulsan 44919, Republic of Korea
Advisor: Professor Mi Hee Lim

Mar. 2011 – Feb. 2015 **B.S., Nano-bioscience and Chemical Engineering, UNIST**, Ulsan 44919, Republic of Korea

Honors, Awards, and Scholarships

July 2016 Poster Award in the Bioinorganic Symposium
May 2016 – Feb. 2017 IBS Seed Research Fellowship in Soft and Living Matter
Mar. 2015 – Apr. 2016 UNIST RA/TA Fellowship

Publications

1. Jeffrey S. Derrick, Richard A. Kerr, Kyle J. Korshavn, Michael McLane, Juhye Kang, **Eunju Nam**, Ayyalusamy Ramamoorthy*, Brandon T. Ruotolo*, and Mi Hee Lim*
"The Importance of the Dimethylamino Functionality on a Multifunctional Framework for Regulating Metals, Amyloid-β, and Oxidative Stress in Alzheimer's Disease"

   Inorg. Chem. **2016**, *55*, 5000-5013

2. Jong-Seok Park, **Eunju Nam**, Hye-Kyeong Lee, Mi Hee Lim*, and Hyun-Woo Rhee*
"In Vivo Mapping of Subcellular Localized Bilirubin"

   ACS. Chem. Biol. **2016**, 11, 2177-2185

3. Ye Won Choi, Jae Jun Lee, **Eunju Nam**, Mi Hee Lim*, and Cheal Kim*.
"A Fluorescent Chemsensor for Al^{3+} Based on Julolidine and Tryptophan Moieties"

   Tetrahedron, **2016**, *72*, 1998-2005.

4. Jae Jun Lee, Yong Sung Kim, **Eunju Nam**, Sun Young Lee, Mi Hee Lim*, and Cheal Kim*
"A PET-based Fluorometric Chemosensor for Determination of Mercury(II) and pH, and Hydrolysis Reaction-Based Colorimetric Detection of Hydrogen Sulfide"

   Dalton Trans. **2016**, *45,* 5700-5712

5. Tae Geun Jo, Jae Jun Lee, **Eunju Nam**, Kwon Hee Bok, Mi Hee Lim*, and Cheal Kim*

"A Highly Selective Fluorescent Sensor for the Detection of Al^{3+} and CN^- in Aqueous Solution: Biological Applications and DFT Calculations"

New J. Chem. **2016**, *40*, 8918-8927

6. Shin Jung C. Lee†, **Eunju Nam**†, Hyuck Jin Lee, Masha G. Savelieff, and Mi Hee Lim*
"Towards an Understanding of Amyloid-β Oligomers: Characterization, Toxicity Mechanisms, and Inhibitors"

Chem. Soc. Rev. **2017**, In Press (DOI: 10.1039/C6CS00731G).

Selected Presentations

1. **Poster, 16th Summer Bioinorganic Chemistry Symposium, Suanbo, Korea, July 18, 2016**
Eunju Nam, Jeffrey S. Derrick, Shin Jung C. Lee and Mi Hee Lim
"A Structure–Activity Relationship of Dopamine toward Metal-Free and Metal-Associated Amyloid-β"

2. **Poster, 17th Yeongnam Region Chemistry Symposium, Pusan, Korea, August 28, 2015**
Eunju Nam, Jeffrey S. Derrick, and Mi Hee Lim*
"Understanding the Role and Function of Catecholamine Transmitters in Alzheimer's Disease"

3. **Poster, 15th Summer Bioinorganic Chemistry Symposium, Suanbo, Korea, July 11, 2015**
Eunju Nam, Jeffrey S. Derrick, and Mi Hee Lim
"Understanding the Role and Function of Catecholamine Transmitters in Alzheimer's Disease"